iScience

CellPress
OPEN ACCESS

Article

Glial regulators of ions and solutes required for specific chemosensory functions in *Caenorhabditis elegans*

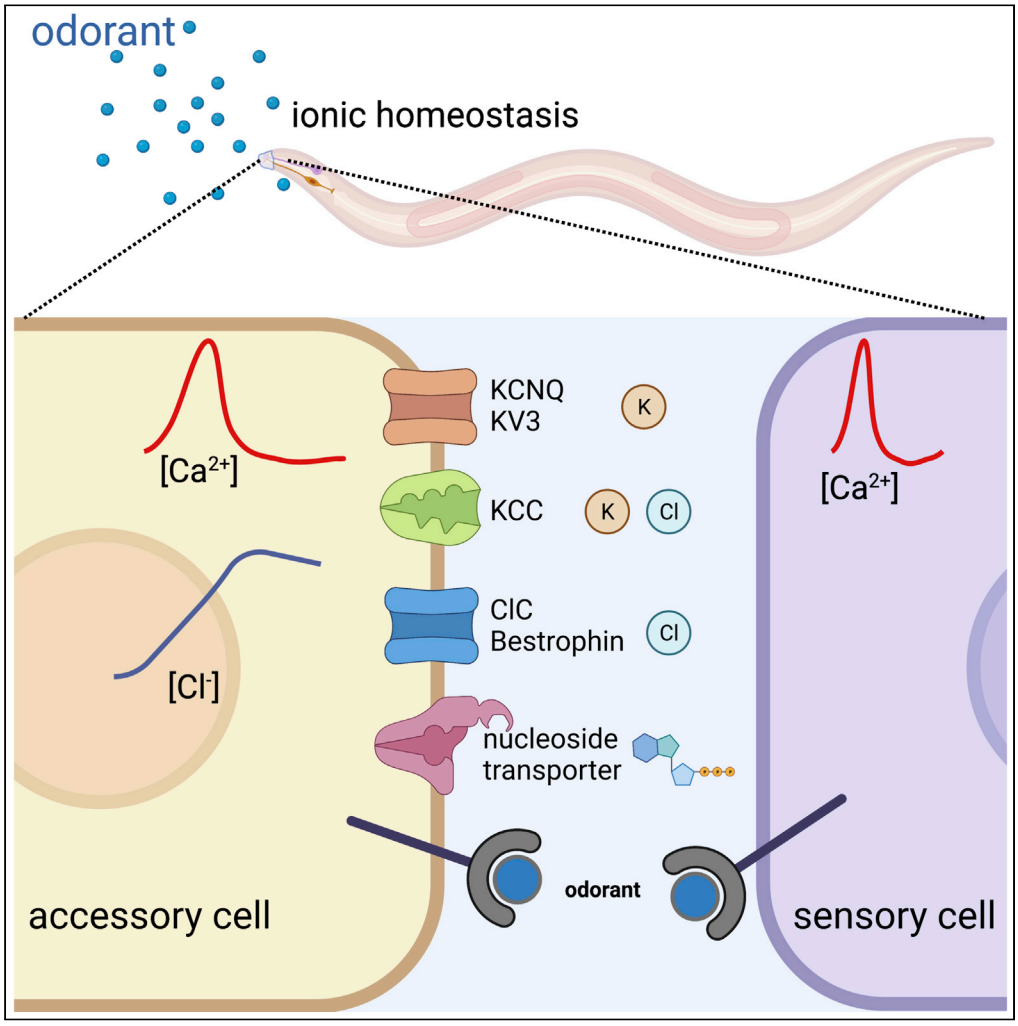

Lei Wang, Bianca Graziano, Nicole Encalada, Jesus Fernandez-Abascal, Daryn H. Kaplan, Laura Bianchi

lbianchi@med.miami.edu

Highlights

Glial regulators of K^+, Cl^-, and nucleosides control olfaction and taste in *C. elegans*

Glial changes in intracellular Ca^{2+} and Cl^- are dependent on these regulators

Glial changes in intracellular Ca^{2+} drive behavioral output

Neuronal output is altered in a unique way by loss of each regulator

Wang et al., iScience 25, 105684
December 22, 2022
https://doi.org/10.1016/j.isci.2022.105684

iScience

CellPress
OPEN ACCESS

Article

Glial regulators of ions and solutes required for specific chemosensory functions in *Caenorhabditis elegans*

Lei Wang,[1] Bianca Graziano,[1] Nicole Encalada,[1,2] Jesus Fernandez-Abascal,[1,3] Daryn H. Kaplan,[1] and Laura Bianchi[1,4,*]

SUMMARY

Glia and accessory cells regulate the microenvironment around neurons and primary sensory cells. However, the impact of specific glial regulators of ions and solutes on functionally diverse primary cells is poorly understood. Here, we systemically investigate the requirement of ion channels and transporters enriched in *Caenorhabditis elegans* Amsh glia for the function of chemosensory neurons. Although Amsh glia ablated worms show reduced function of ASH, AWC, AWA, and ASE neurons, we show that the loss of glial enriched ion channels and transporters impacts these neurons differently, with nociceptor ASH being the most affected. Furthermore, our analysis underscores the importance of K^+, Cl^-, and nucleoside homeostasis in the Amphid sensory organ and uncovers the contribution of glial genes implicated in neurological disorders. Our findings build a unique fingerprint of each glial enriched ion channel and transporter and may provide insights into the function of supporting cells of mammalian sensory organs.

INTRODUCTION

Sensory apparati across species are composed of primary sensory cells and accessory cells, including glia. For example, the mammalian olfactory epithelium is composed of olfactory sensory neurons and supporting microvillar and sustentacular cells, in addition to immature neurons and basal stem cells. Microvillar and sustentacular cells are intimately associated with the olfactory neurons, enwrapping their cell body, and have been suggested to provide physical, metabolic, and ionic support to the olfactory sensory neurons.[1–5] Similarly, in the mammalian taste buds, glial-like type I cells have cytoplasmic lamellae that ensheath the type II and type III cells that mediate detection of tastants in the oral cavity. Type I cells participate in transmitter clearance[6,7] and regulate the concentration of K^+ and Cl^- in taste buds.[8–10] Furthermore, type I cells have been recently shown to respond to ATP released by type II cells with an increase of intracellular Ca^{2+}, suggesting that they may release gliotransmitters.[11]

The functional role of the olfactory supporting cells has been recently brought to the forefront by the COVID-19 pandemic. Indeed, anosmia is one of the earliest, most prevalent, and long-lasting symptoms of SARS-CoV-2 infection, affecting up to 85% of infected individuals.[12] Intriguingly though, the SARS-CoV-2 virus primarily infects the olfactory supporting microvillar and sustentacular cells that express the viral entry proteins ACE2 and TMPRSS2,[13–15] suggesting that those accessory cells are crucial for olfaction. Despite data demonstrating that supporting cells of the chemosensory apparatus are essential for function, little is known about the molecular mechanisms underlying the contribution of these cells to sensory perception.

C. elegans responds to odorants and tastants primarily via the amphid sensory organ. This is a bilateral organ located in the head of the worm, which is composed of 12 pairs of sensory neurons, ten of which are chemosensory neurons, and two pairs of supporting glial cells called the amphid sheath (Amsh) and the amphid socket (Amso) cells. Cell ablation studies and studies using mutants have shown that Amsh cells are needed for the structure and/or function of the amphid sensory neurons.[16–22] Exciting recent work has also shown that the Amsh cells directly respond to odorants and touch via the activation of cell autonomous receptors and intracellular signaling.[23,24]

[1]Department of Physiology and Biophysics, University of Miami Miller School of Medicine, Rm 5133 Rosenstiel Building, 1600 NW 10th Avenue, Miami, FL33136, USA

[2]Present address: HCW Biologics, Miramar, FL 33025, USA

[3]Present address: Andalusian Centre for Developmental Biology (CABD), CSIC-Universidad Pablo deOlavide, Carretera deUtrera, km 1 41013 Seville – Spain

[4]Lead contact

*Correspondence: lbianchi@med.miami.edu

https://doi.org/10.1016/j.isci.2022.105684

A

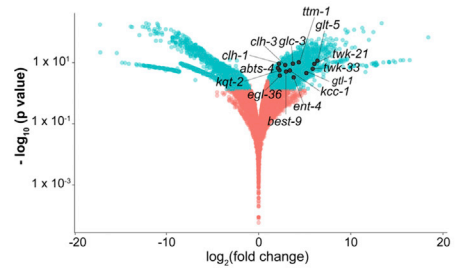

B

C.elegans gene name	Function	Human homology
abts-4	Anion/bicarbonate Transporter	SLC4A1, SLC4A2, SLC4A3
best-9	Bestrophin (Chloride channel)	BEST1, BEST2, BEST4
clh-1	CLC-type chloride channel	CLCN2, CLCNKA, CKCNKB
clh-3	CLC-type chloride channel	CLCN2, CLCNKA, CKCNKB
egl-36	Voltage-gated K^+ channel	KCNC1, KCNC2, KCNC4
ent-4	Equilibrative nucleoside transporter	SLC29A1, SLC29A2, SLC29A3
glc-3	Glutamate-gated Cl^- channel	GLRA1
glt-5	Glutamate transporter	SLC1A2
gtl-1	TRP cationic channel	TRPM1, TRPM3, TRPM7
kqt-2	Voltage-gated K+ channel	KCNQ1
kcc-1	K^+/Cl^- co-transporter	SLC12A4, SLC12A6, SLC12A7
twk-21	Two-pore domains K^+ channel	KCNK16, KCNK17, KCNK5
twk-33	Two-pore domains K^+ channel	KCNK16, KCNK17, KCNK5
ttm-1	Zinc transporter	SLC30A3, SLC30A8

C

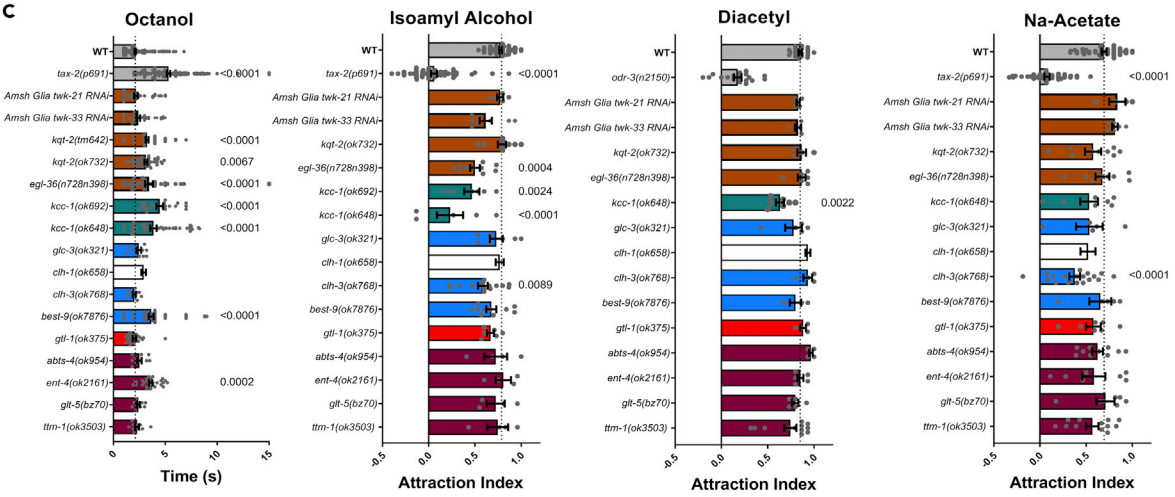

D

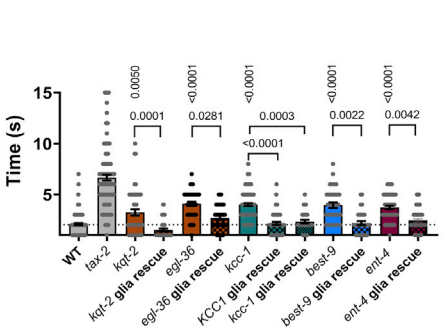

E

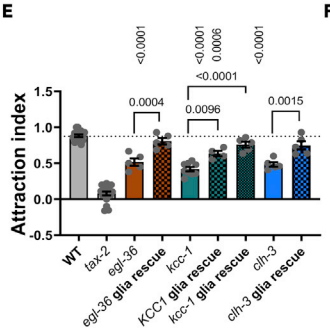

F

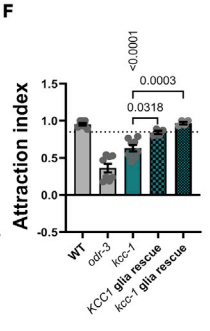

G

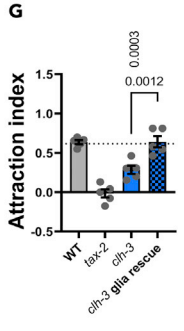

H

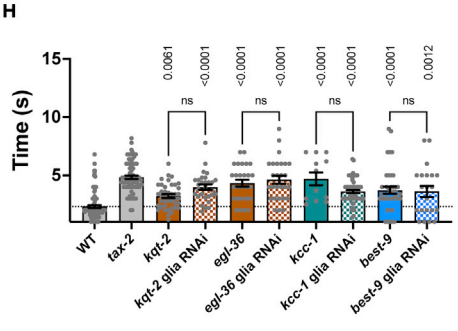

I

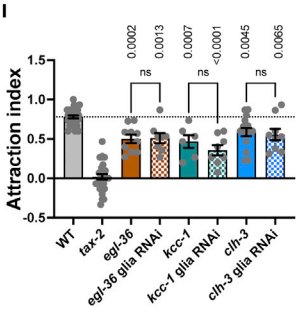

J

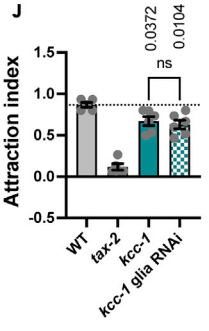

K

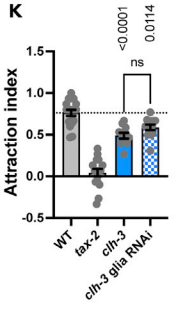

Figure 1. Specific Amsh cells' channels and transporters are required for chemotaxis

(A) The volcano plot of RNA-sequencing data shows the expression of all the genes in Amsh cells compared to the other *C. elegans* cells.[20] The genes with a $p < 0.05$ and $\log_2$ fold change larger than +/− 1 are labeled in cyan. The genes with a $p > 0.05$ or $\log_2$ fold change smaller than +/− 1 are labeled in red. The enriched ion channel and transporter genes studied here are labeled in black.

(B) The table of enriched ion channel and transporter genes, their function, and their human homologs.

(C) Chemotaxis assay of mutant strains for the genes shown in Figure 1B. Time to response to the odorant octanol (10%) in seconds (n = 10 to 270), attraction index to isoamyl alcohol (1:1000) (n = 4 to 55), diacetyl (1:1000) (n = 4 to 19), and Na-acetate (0.2 M) (n = 4 to 47) for all the mutant strains. Positive and negative controls were wild type (WT) and *tax-2(p691) or odr-3(n2150)*. The K^+ channel genes (*twk-21*, *twk-33*, *kqt-2*, and *egl-36*) are shown in brown, the K^+/Cl^- transporter gene (*kcc-1*) is shown in green, the Cl^- channel genes (*clh-1*, *clh-3*, and *best-9*) are shown in blue, the cation channel gene (*gtl-1*) is shown in red, and the solute carrier genes (*abts-4*, *ent-4*, *glt-5*, and *ttm-1*) are shown in magenta. *clh-1*data were published and are shown in white.[24]

(D) Time to response to octanol (10%) (n = 33 to 90), (E) attraction index to isoamyl alcohol (n = 4 to 13), (F) attraction index to diacetyl (n = 4), and (G) attraction index to Na-acetate (n = 5) of the mutants (solid color columns) and Amsh glia specific rescues (checkered columns) as shown.

(H) Time to response to octanol (10%) (n = 12 to 104), (I) attraction index to isoamyl alcohol (n = 6 to 30), (J) attraction index to diacetyl (n = 6) and (K) and attraction index to Na-acetate (n = 11 to 18) of the mutants (solid color columns) and Amsh glia specific knockdown (checkered columns) as indicated.

Individual data points as well as means +/− SE are shown in each panel. p values were calculated by ANOVA with Tukey's correction. For attraction to isoamyl alcohol, diacetyl, and Na-acetate ~30 animals were tested in each experiment to determine the attraction index. For octanol avoidance the number indicates the number of animals tested.

Despite great progress in understanding the function of the worm Amsh, much remains to be learned and leveraged to gain insights into the function of supporting cells in the mammalian chemosensory organs. Moreover, the glia/neuron crosstalk occurring in this sensory apparatus of the worm can model glia/neuron cross talk in other parts of the nervous system across species. Toward this goal, in the past we have taken the unbiased approach of RNA sequencing, identifying ~1000 Amsh glial enriched transcripts.[20,24] Here, we focus on glial ion channel and transporter genes identified in that study as they are excellent candidates to mediate mechanisms of glia/neuron cross talk, including control of the microenvironment surrounding the sensory neurons. This approach led recently to the identification of glial ClC Cl^- channel CLH-1 as a major regulator of nose touch response in *C. elegans*.[24] Using behavioral assays, Ca^{2+} imaging, and pharmacological approaches, we present here an analysis of the role of 13 additional Amsh cell enriched genes in chemosensory function. These genes include the *clh-1* homolog *clh-3*, voltage-gated and two pore domain K^+ channels, a bestrophin gene, a K^+/Cl^- cotransporter, a glutamate transporter, a glutamate-gated channel, a TRP channel, and transporters of bicarbonate, zinc, and nucleoside. We show how the loss of these genes in glia causes distinct effects on glia and sensory neurons, suggesting their specific roles in glia/neuron cross talk in chemosensation.

RESULTS

Loss of specific Amsh channels and transporters causes chemosensory deficits

Glia regulate neuronal function by control of ions and solutes, including neurotransmitters and neuropeptides, in the extracellular environment. Thus, in our small-scale screen, we focused on genes that encode plasma membrane ion channels and transporters, which are likely involved in these processes (Figure 1A). We found that Amsh are enriched in transcripts encoding for transporters of bicarbonate, Cl^-, K^+, glutamate, Zn^{2+}, and nucleosides, as well as channels permeable to K^+, Cl^-, and cations (Figure 1B). A review of three other RNA sequencing and DNA microchip databases confirm that these transcripts are expressed in Amsh glia across development in *C. elegans*, supporting that these genes function in these cells[16,25,26] (Figure S1). Amsh glia are also enriched in several innexin transcripts and express many more channels and transporters, but those were not studied here (Figure S2).

To determine whether these genes are needed for chemosensory function in *C. elegans*, we performed behavioral assays on mutants. We selected the aversive odorant octanol, the attractive odorants isoamyl alcohol and diacetyl, and Na-acetate to test the function of polymodal nociceptors ASH, chemosensory neurons AWC and AWA, and salt sensing neurons ASE and to a lesser extent ASG, respectively.[27–29] For the two-pore domain channels *twk-21* and *twk-33*, mutants were not available, so we resorted to using Amsh glia specific RNAi. We found that although some of the mutants displayed chemosensory deficits when tested with these odorants, others behaved like wild type (Figure 1C). More specifically, mutants of the K^+ channels *kqt-2* (two independent alleles) and *egl-36*, the K^+/Cl^- cotransporter *kcc-1* (two independent alleles), the Cl^- channel *best-9*, and the nucleoside transporter *ent-4* displayed reduced aversive response to octanol. *egl-36*, *kcc-1*, and the Cl^- channel *clh-3* displayed reduced chemotaxis to isoamyl alcohol. Finally, *kcc-1* and *clh-3* showed reduced attraction to diacetyl and Na-acetate, respectively.

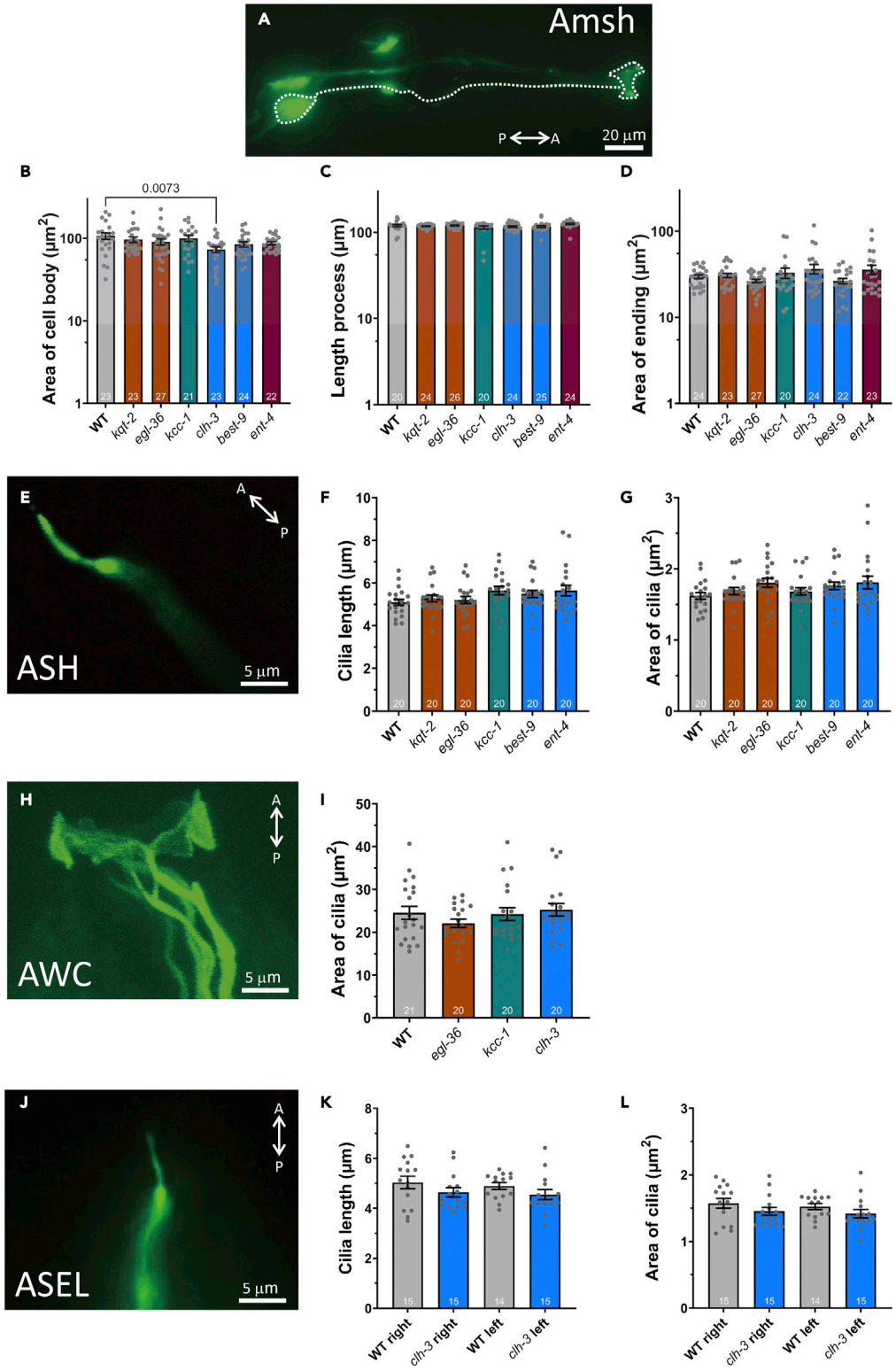

Figure 2. No changes in the morphology of Amsh glia and amphid sensory in channel and transporter mutants

(A) A florescence image showing Amsh cells expressing GCamP-6s under the control of the Amsh specific promoter *T02B11.3*.[16] The cell body, process, and ensheathing glial ending are shown by the dotted line. The size bar corresponds to 20 µm.

Figure 2. *Continued*

(B–D) The area of cell body, length of process, and area of ensheathing endings, respectively, of Amsh cells in WT, *kqt-2*, *egl-36*, *kcc-1*, *clh-3*, *best-9*, and *ent-4* mutant worms.

(E) A confocal image of the cilium of an ASH neuron in a wild type worm.

(F–G) The length and area of ASH neuron's cilia in wild type and mutants with reduced octanol avoidance.

(H) A confocal image of the cilium of an AWC neuron in a wild type worm.

(I) The area of the cilia of AWC neurons in wild type and mutants with reduced attraction to isoamyl alcohol *egl-36*, *kcc-1*, and *clh-3* worms.

(J) The cilium of an ASEL neuron in a wild type worm.

(K–L) The length and area of the cilium of an ASER and ASEL neuron is shown for WT and *clh-3* mutant as indicated. A represents anterior, P represents posterior. Data are shown as individual data points as well mean ± SE. The size bars for e, h, and j correspond to 5 μm p values were calculated by ANOVA with Tukey's correction. n is shown in the columns.

These results show that more mutants had altered response to octanol and isoamyl alcohol than diacetyl and Na-acetate. However, using worms in which Amsh glia were genetically ablated, Bacaj et al. showed that ASH, AWC, AWA, and ASE neurons all require Amsh glia for function,[16] which we confirmed under our experimental conditions (Figures S3A-S3D). These results suggest the requirement of different ions and solutes' regulators for distinct sensory functions. To further test this idea, we assayed nose touch response, which is primarily mediated by nociceptor ASH, in *kqt-2(ok732)* (the *kqt-2* allele used from here onward given the similarity in the behavioral responses between the two alleles), *egl-36*, *best-9*, *kcc-1(ok648)* (the *kcc-1* allele used from here onward given the similarity in the behavioral responses between the two alleles), and *ent-4* mutants, all of which display reduced response to the aversive odorant octanol (Figure 1C). We added *clh-1* mutants as control, as we recently showed that this channel is needed in Amsh glia for nose touch responses.[24] We found that these 5 mutants responded to nose touch just like wild type (Figure S3E). Conversely, *clh-1* mutants respond normally to octanol but are severely nose touch insensitive (Figures 1C and S3E).[24] These results support the idea that each function requires the activity of specific regulators of ionic and solute homeostasis in the *C. elegans* Amphid sensory organ. Our results also confirm that ablation of the Amsh glia has more global effects than the knockout of individual regulators of ion/solute transport.

To determine whether it is the loss of these channels and transporters in Amsh glia that causes the chemosensory phenotype, we performed experiments in cell specific rescue and RNAi strains. We found that all the chemosensory phenotypes were rescued by expression of the corresponding wild type cDNA in Amsh glia (Figures 1D–1G) and were recapitulated by Amsh glia knockdown (Figures 1H–1K). In the case of K^+/Cl^- cotransporter *kcc-1*, which is required for three distinct sensory behaviors, we also used human KCC1 for the rescue experiments. We found that human KCC1 rescues, albeit not as well as the worm KCC-1, the *C. elegans* chemosensory deficits when expressed in Amsh glia of *kcc-1* mutants, supporting conservation of function across species (Figures 1D–1F). To conclude, K^+ channels *kqt-2* and *egl-36*, the K^+/Cl^- cotransporter *kcc-1*, Cl^- channels *best-9* and *clh-3*, and the nucleoside transporter *ent-4* are needed in Amsh glia for distinct chemosensory functions (Figure 8). Given that we have not tested the response of these mutants to all sensory stimuli, it remains possible that the mutants that did not show any chemosensory or touch deficits in our assays are defective in other sensory modalities including response to temperature, UV light, sound, and electric fields.[30–34] Nevertheless, we focused the rest of our study on the mutants with reduced response to octanol, isoamyl alcohol, diacetyl, and Na-acetate.

Normal morphology of glia and neurons in chemosensory mutants

We next wondered whether chemosensory deficits in channel and transporter mutants were caused by abnormal morphology of glia or sensory neurons.[16] We thus measured the sizes of glia and neurons in mutants expressing GFP in these cells. For Amsh glia, we measured the size of the cell body, the length of the cellular process, and the area of the ensheathing ending in the mutants (Figures 2A–2D). We found no major morphological difference among the mutants, except for a slightly smaller Amsh cell body in *clh-3* worms, supporting that these channels are not involved in establishing or maintaining Amsh glia morphology. The smaller cell body size observed in *clh-3* worms is likely because of the overall small size of these mutants (Figures S4A and S4B). Of interest, we did not find any difference in length of the Amsh cellular process in *clh-3* despite their shorter body (Figure 2C). Closer inspection of the cellular processes revealed that they have more bends in *clh-3* than in wild type, possibly explaining this discrepancy (Figures S4C and S4D). Moreover, *clh-3* mutants respond normally to octanol and diacetyl suggesting that not all the functions of the Amsh glia are lost in these mutants. A shorter body, but not as short as in *clh-3*

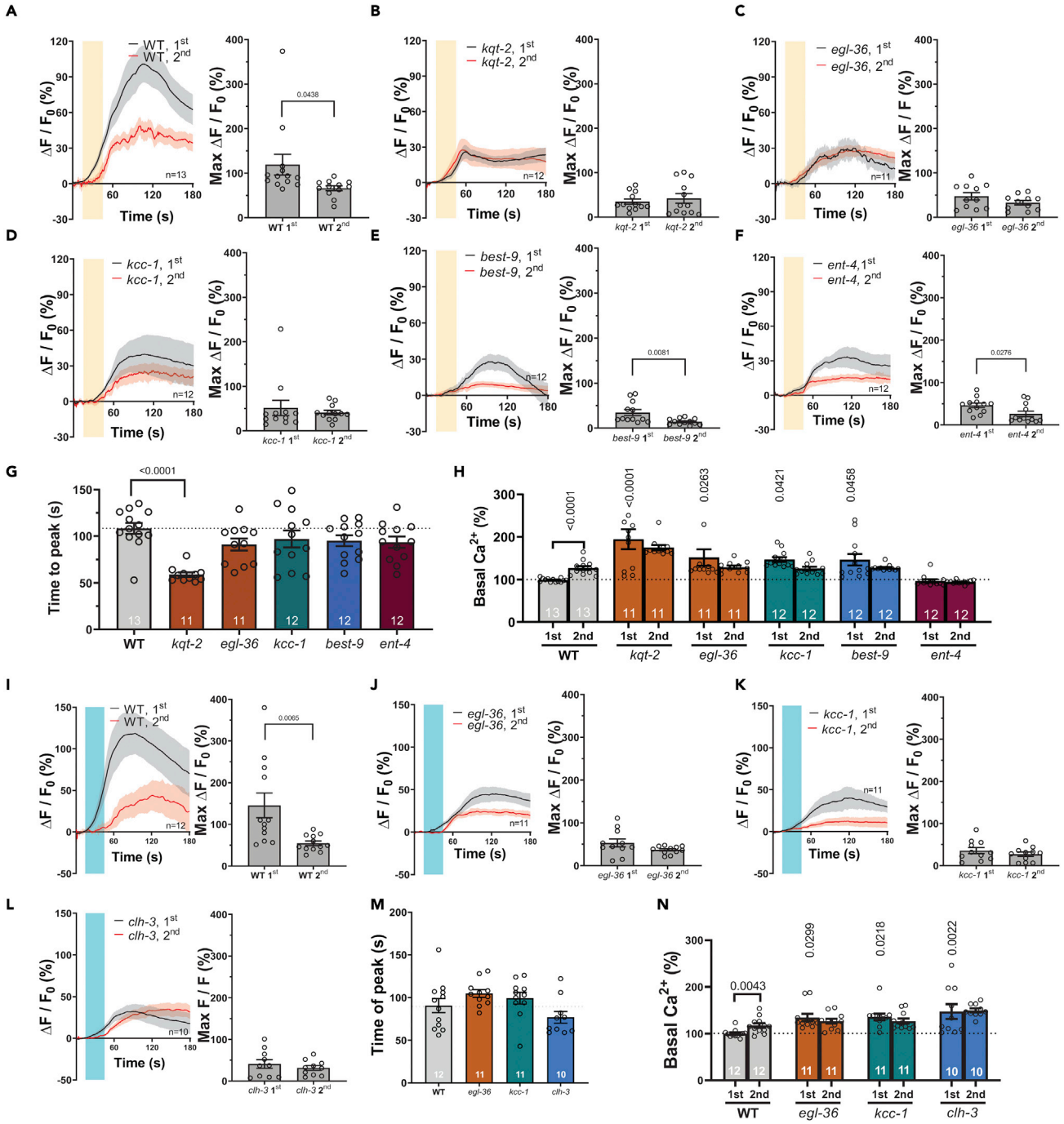

Figure 3. Glial channels and transporters needed for chemotaxis are required for the function of Amsh cells

(A–F) Calcium transients generated in Amsh by perfusion with octanol (1:1,000, yellow shaded area) as measured by % increase of GCaMP-6s fluorescence above the baseline ($\Delta F/F_0$) in wild type and mutants with reduced octanol avoidance *kqt-2*, *egl-36*, *kcc-1*, *best-9*, *and ent-4* for the first stimulation (black) and second stimulation (red) (left panels). The right panels show the peak percentage of GCaMP-6s ($\Delta F/F_0$). n is shown within each left panel.

(G) Average time to peak in seconds of octanol induced Ca^{2+} transients for the indicated strains.

(H) The relative to wild type basal calcium levels of Amsh glia for the indicated strains. For g and h, the n is indicated in the columns.

Figure 3. *Continued*

(I–L) Calcium transients generated in Amsh by perfusion with isoamyl alcohol (1:100, cyan shaded area) as measured by % increase of GCaMP-6s fluorescence above the baseline ($\Delta F/F_0$) in wild type, and mutants with reduced isoamyl alcohol avoidance *egl-36*, *kcc-1*, and *clh-3* for the first stimulation (black) and second stimulation (red). The right panels show the peak percentage of GCaMP-6s $\Delta F/F_0$. n is shown in each left panel.

(M) Average time to peak in seconds of isoamyl alcohol induced Ca^{2+} transients for the indicated strains.

(N) The relative to wild type basal calcium levels of Amsh glia for the indicated strains. The n is indicated in the columns. Data are shown as mean ± SE. p values are shown in the panels and were obtained by unpaired Student's t-test or in the case of panels g h, m, and n by ANOVA with Tukey's correction.

mutants, was also observed in *kcc-1* mutants, but not in all the other mutants analyzed here (Figures S4A and S4B). For the neurons, we focused on the cilia, which are the terminal dendrites that house transduction molecules (Figures 2E-2L).[35–38] We did not find any gross abnormality in the morphology or size of the cilia of ASH, AWC, or ASE neurons in these mutants, despite our experimental setup being able to detect ~25% change in the size of the cilia in animals reared on hypertonic plates containing α-methyl-D-glucopyranoside (NMG) (Figures S4E-S4G). AWA neurons could not be analyzed because of the low GFP expression in *odr-10*:GFP (kyIs53 X) transgenics (image not shown).[39] In conclusion, although we cannot exclude submicroscopic changes, our data support that *kqt-2*, *egl-36*, *kcc-1*, *best-9*, and *ent-4* are needed for the function rather than the overall structure of Amsh glia and the sensory neurons (Figure 8).

Reduced response of glia to odorants in chemotaxis mutants

Amsh glia respond to odorants and touch by rise in intracellular Ca^{2+}.[23,24] We thus wondered whether the channels and transporters needed for chemosensory function were also needed for Amsh glial Ca^{2+} transients in response to exposure to odorants. We focused on responses to octanol and isoamyl alcohol, as in behavioral assays they show the requirement of multiple channels and transporters. Thus, we monitored *in vivo* intracellular Ca^{2+} in wild type and mutant animals expressing GCaMP-6s in Amsh glia. In wild type animals, we found robust and slow Ca^{2+} transients upon exposure to 1:1000 octanol, which were reduced in amplitude upon exposure with the odorant a second time (Figure 3A). These results are consistent with previously published data and support that Amsh glia respond to and adapt to octanol.[23] When we imaged *kqt-2*, *egl-36*, *kcc-1*, *best-9*, and *ent-4* mutants we found that the Ca^{2+} transients in response to exposure to octanol were smaller than in wild type, consistent with the reduced response of these mutants in behavioral assays (Figures 3B-3F and S5A). However, there were some notable differences between the mutants. First, adaptation was not seen in *kqt-2*, *egl-36*, and *kcc-1* mutants, but was still present in *best-9* and *ent-4* mutants. Second, the time to peak was faster in *kqt-2* mutants as compared to wild type and the rest of the mutants (Figure 3G). These results suggest that *kqt-2*, *egl-36*, *best-9*, and *ent-4* are needed for different aspects of regulation of Amsh glial intracellular Ca^{2+} rise upon exposure to octanol (Figure 8).

To confirm, as reported by Chen et al.,[40] that the rise of intracellular Ca^{2+} in Amsh glia is mediated by activation of L-type voltage-gated Ca^{2+} channels, we monitored intracellular Ca^{2+}upon exposure with octanol in animals pre-treated with the L-type channel blocker nifedipine. We found that Ca^{2+} transients were completely suppressed in these animals (Figure S6A). Because of its voltage dependence, a depolarized membrane potential is expected to cause chronic activation of L-type Ca^{2+} channels with consequent rise of intracellular Ca^{2+} at baseline. Given that *kqt-2*, *egl-36*, *best-9*, and *kcc-1* are regulators of the flux of K^+ and Cl^- ions across the membrane, and thus may directly or indirectly influence the resting membrane potential, we asked whether intracellular Ca^{2+} at baseline was altered in these mutants. To answer this question, we quantified GCaMP-6s fluorescence at baseline as a measure of intracellular Ca^{2+} concentration. We found that indeed intracellular Ca^{2+} was higher in *kqt-2*, *egl-36*, *best-9*, and *kcc-1* as compared to wild type (Figure 3H). Knock-out of the equilibrative nucleoside transporter *ent-4* does not change intracellular Ca^{2+}, consistent with the fact that this is not an ion transporter and thus is not expected to influence the membrane potential.[41] Of interest, although in WT intracellular basal Ca^{2+} is higher before the second exposure to octanol as compared to the first one, in the mutants it is at the same level (Figure 3H). This is consistent with the idea that the mutants might be already in an adapted state even before the first stimulation with octanol.

When we monitored the Amsh glia response to 1:100 isoamyl alcohol in wild type, we also found slow robust Ca^{2+} transients that adapted upon second exposure with the odorant, which was again consistent with published work (Figure 3I).[23] Analysis of *egl-36* and *kcc-1* mutants yielded results like the ones obtained in animals perfused with octanol, though a tendency to adaptation persisted, perhaps as a result of the higher concentration of odorant used in these experiments (Figures 3J,3K, and S5B). Similarly, *clh-3* mutants displayed smaller Ca^{2+} transients and no statistical difference in the amplitude of Ca^{2+} transients

between the first and second exposure to isoamyl alcohol (Figures 3L, S5B, and 8). Time to peak was not statistically different than wild type in any of the mutants (Figure 3M). But *egl-36*, *kcc-1*, and *clh-3* mutants all displayed higher intracellular Ca^{2+} at baseline prior to the first and second exposure to isoamyl alcohol as compared to wild type, again suggesting that they either directly or indirectly, influence the membrane potential of Amsh cells (Figure 3N). On the contrary, in wild type intracellular Ca^{2+} is statistically higher prior to the second exposure to isoamyl alcohol than it is prior to the first one, as shown for octanol (Figure 3N). Finally, we tested the response of Amsh glia to 0.5, 1, and 2 M Na-acetate and found no changes in intracellular calcium (Figures S6B-S6D). This is consistent with findings by Duan et al. and suggest that Amsh glia are likely insensitive to changes in extracellular Na^+ concentration.[23] To conclude, our analysis of Amsh glia response to octanol and isoamyl alcohol reveals that K^+ channels *kqt-2* and *egl-36*, Cl^- channels *best-9* and *clh-3*, the K^+/Cl^- cotransporter *kcc-1*, and the nucleoside transporter *ent-4* are all needed for the generation of Ca^{2+} transients and for cellular adaptation in these cells upon exposure to odorants.

To determine whether changes in intracellular Ca^{2+} in Amsh glia correlate with animal behavior, we knocked down the L-type Ca^{2+} channel *egl-19* in these cells and then monitored behavioral responses. As expected, RNAi of *egl-19* in Amsh glia, leads to smaller Ca^{2+} transients upon exposure to octanol and isoamyl alcohol (Figures S6E-S6H).[40] Importantly, *egl-19* Amsh glia RNAi animals respond less to both octanol and isoamyl alcohol (Figures S6I and S6J). The change in morphology of glia seen in *egl-19* mutants was not observed in RNAi experiments, probably because of residual EGL-19 activity[40] (Figure S6K). Taken together, these results are consistent with the idea that changes in intracellular Ca^{2+} in Amsh glia correlate with animal behavior.

Our results show that mediators of K^+ and Cl^- transport across the Amsh cells plasma membrane are required for chemotaxis in *C. elegans*. We wondered whether mediators of transport of the same ion act within the same molecular pathway. To test this idea, we exploited the concept of genetic epistasis by which knockout or knockdown of two genes within the same pathway leads to a phenotype like the one caused by the individual mutations. We thus built *kqt-2;egl-36* RNAi, *best-9;kcc-1* RNAi, and *clh-3;kcc-1* double mutants, and tested whether their chemotaxis phenotype was similar to or worse than the single mutants. In all three strains, we found that the chemotaxis phenotype was like that of single mutants (Figure S7). Even though we cannot rule out the possibility that RNAi may lead to incomplete elimination of the expression of the genes, these results suggest that *kcc-1*, *clh-3*, and *best-9* on the one hand and *egl-36* and *kqt-2* on the other act within the same molecular pathways to orchestrate responses to the odorants octanol and isoamyl alcohol.

Chloride changes in glia in response to odorants

We published that Amsh glia undergo changes in intracellular Cl^-upon touch stimulation.[24] To determine whether Cl^- concentration changes in Amsh glia upon exposure to odorants too, we monitored fluorescence changes in Amsh glia expressing SuperClomeleon. We found robust and slow rise in intracellular Cl^- in Amsh glia of wild type upon exposure with octanol (Figure S8A). Of interest, although the second touch stimulation causes a decrease of intracellular Cl^- in Amsh glia, which we showed is mediated by Cl^- efflux via the CLH-1 channel,[24] the second exposure to octanol still causes an increase in Cl^- concentration (Figures S8A and S8D). When we monitored Cl^- changes in Amsh glia of the Cl^- channel and transporter mutants *best-9* and *kcc-1*, we found similar results, though the second exposure to the odorant caused adaptation (Figures S8B-S8D). Isoamyl alcohol also caused raise in intracellular Cl^- in wild type, though to a smaller degree than octanol (Figure S8E). In *clh-3* mutants glial intracellular Cl^- changes were greatly reduced suggesting that CLH-3 may mediate Cl^- influx into glia (Figures S8F and S8H). On the contrary, in *kcc-1* mutants Cl^- changes were robust and showed marked adaptation, similarly to what seen upon perfusion with octanol (Figures S8G and S8H). These results show that Amsh glia undergo changes in intracellular Cl^-upon exposure to odorants and that Cl^- channels and transporter *best-9*, *clh-3*, and *kcc-1* are involved in the regulation of these changes. Changes in intracellular Cl^- concentration in Amsh glia may affect the resting potential of these cells and their Cl^- efflux which we showed plays a key role in GABA signaling from glia to neurons.[24]

Altered Ca^{2+} in ASH neurons of chemotaxis mutants

The response to octanol in the worm is primarily mediated by ASH neurons, with ADL and AWB neurons participating only in the absence of food or when ASH neurons are ablated.[27,42,43] Duan et al. showed

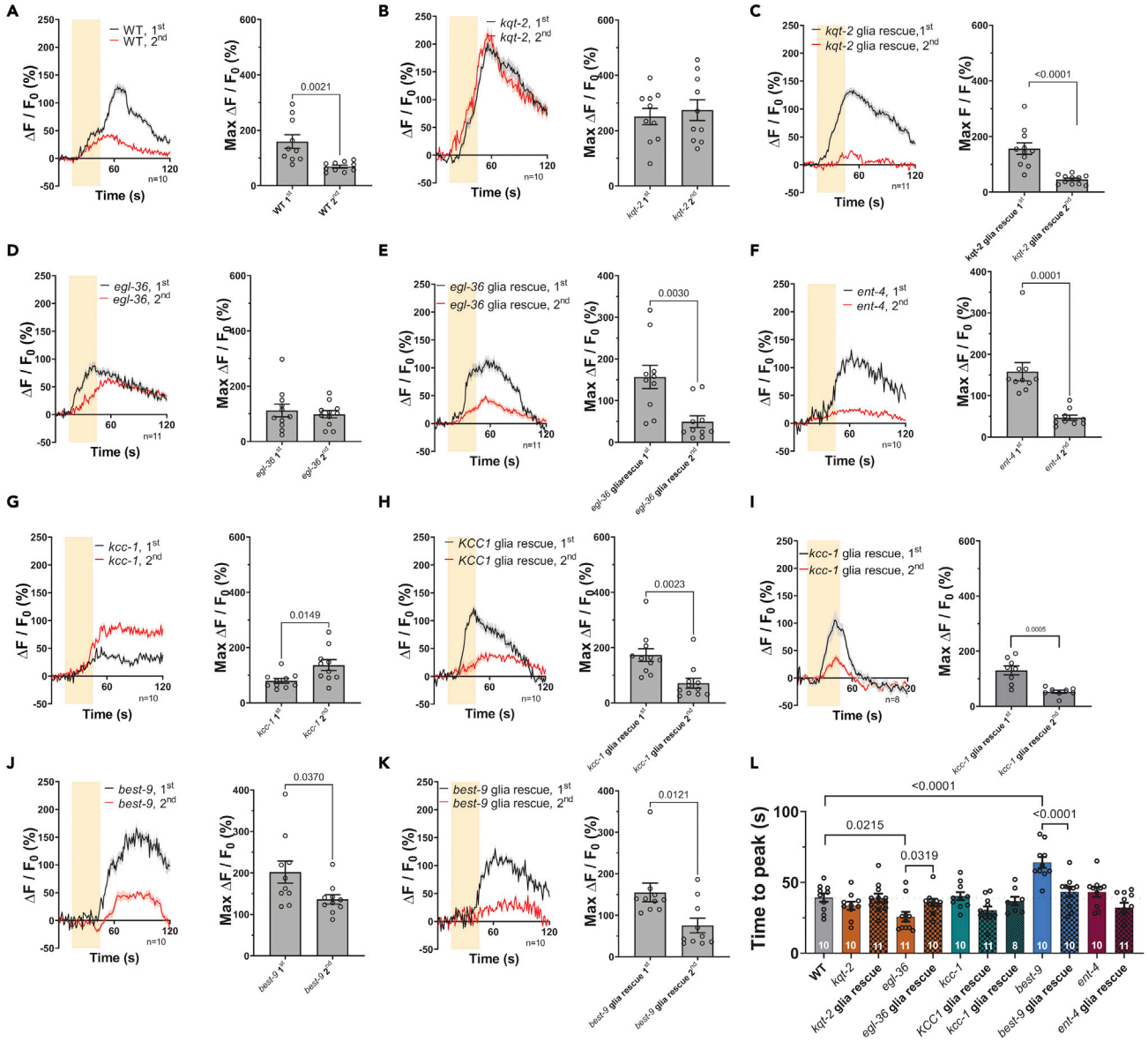

Figure 4. ASH neuronal function in channel and transporter mutants

Calcium transients generated in ASH neurons by perfusion with octanol (1:1,000, yellow shaded area) as measured by % increase of GCaMP-6s fluorescence above the baseline ($\Delta F/F_0$) in (A) wild type and mutants with reduced octanol avoidance and related glia specific rescue strains as follows, (B) *kqt-2*,(C) *kqt-2* glia rescue,(D) *egl-36*,(E) *egl-36* glia rescue, (F) *ent-4*, (G) *kcc-1*,(H) human KCC1 glia rescue in *kcc-1*mutant,(I) worm *kcc-1* glia rescue in *kcc-1*mutant, (J) *best-9*, and (K) *best-9* glia rescue. The first stimulation is in black and second stimulation is in red. The right panels show the peak percentage of GCaMP-6s ($\Delta F/F_0$). N is shown each left panel. (L) Time to peak in seconds of octanol induced Ca^{2+} transients for the indicated strains. The n is sown in each column. Data are shown as mean ± SE. p values are shown in the panels and were obtained by unpaired Student's t-test or in the case of panel L, by ANOVA with Tukey's correction by comparing each mutant with WT. Rescues were compared with the corresponding mutant by t-test.

that Amsh glia regulates ASH neuronal Ca^{2+} transients, in particular their adaptation to consecutive exposures to octanol.[23] We thus hypothesized that together with glial Ca^{2+} transients, ASH neuronal Ca^{2+} transients might also be altered in mutants in response to octanol. Therefore, we monitored Ca^{2+} transients in wild type and mutants expressing GCaMP-6s in ASH neurons.

In wild type ASH neurons, we found robust Ca^{2+} transients upon exposure to 1:1000 octanol. As shown by Duan et al., ASH neurons adapt to a second exposure to octanol and thus display reduced Ca^{2+} transients (Figure 4A).[23] Of interest, despite *kqt-2*, *egl-36*, *kcc-1*, *best-9*, and *ent-4* mutants all showing similar

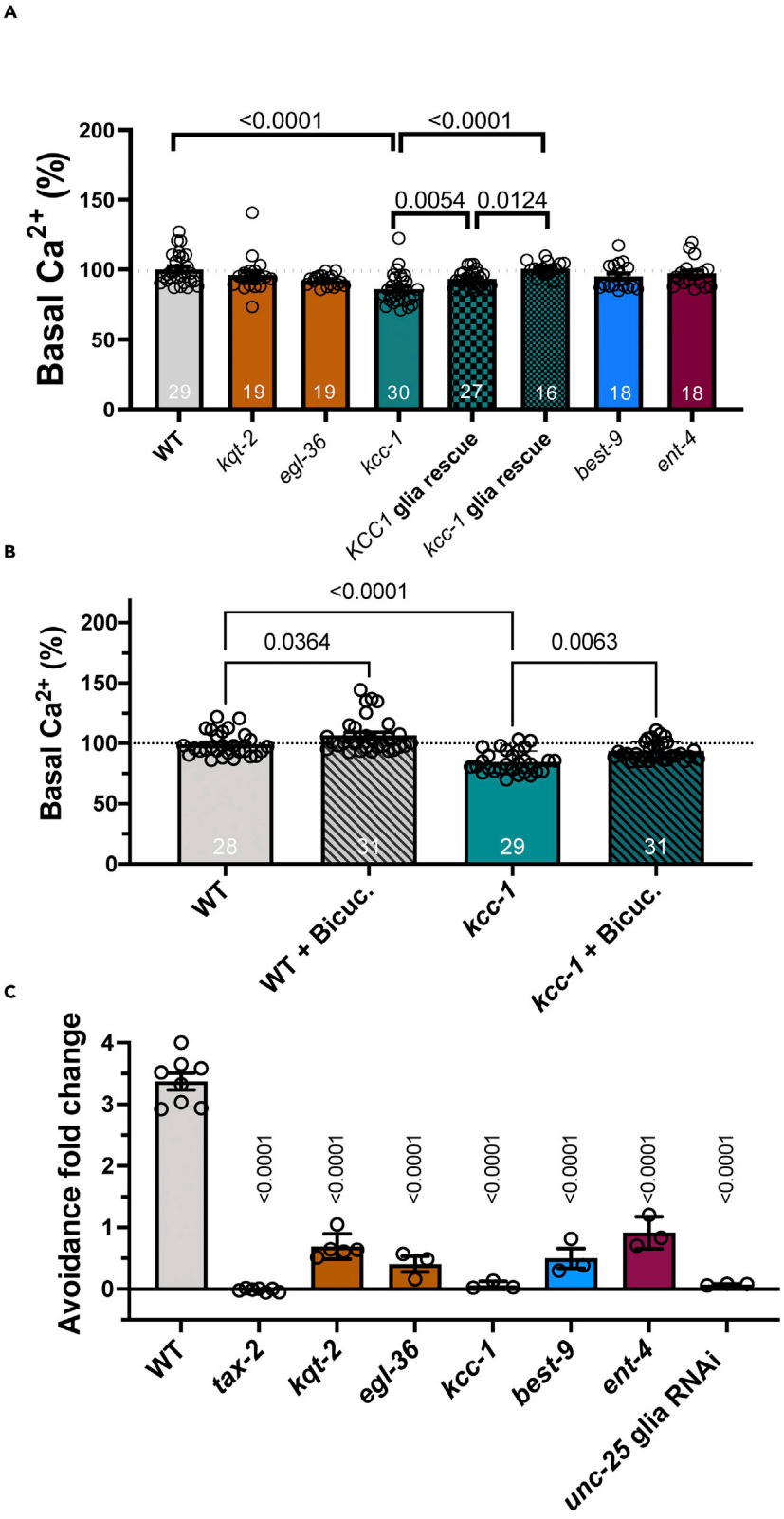
A
Basal Ca2+ (%)
<0.0001
<0.0001
0.0054
0.0124
29
19
19
30
27
16
18
18
WT
kqt-2
egl-36
kcc-1
KCC1 glia rescue
kcc-1 glia rescue
best-9
ent-4
B
Basal Ca2+ (%)
<0.0001
0.0364
0.0063
28
31
29
31
WT
WT + Bicuc.
kcc-1
kcc-1 + Bicuc.
C
Avoidance fold change
<0.0001
<0.0001
<0.0001
<0.0001
<0.0001
<0.0001
<0.0001
WT
tax-2
kqt-2
egl-36
kcc-1
best-9
ent-4
unc-25 glia RNAi

Figure 5. Glial KCC-1 is needed for basal Ca^{2+} in ASH neurons

(A) The relative to wild type basal calcium levels in ASH neurons of the indicated strains which have reduced octanol avoidance: *kqt-2*, *egl-36*, *kcc-1*, human KCC1 glia rescue strain, worm *kcc-1* glia rescue strain, *best-9*, *and ent-4*.

(B) The effect of the $GABA_A$ receptor antagonist bicuculline on the basal calcium of ASH neurons in wild type and *kcc-1* mutants.

(C) Behavioral adaptation to octanol. The time to response to 10% octanol post-adaptation minus the time to response pre-adaptation divided by the time to response pre-adaptation. n = 3 to 8 experiments, with at least 10 worms tested in each experiment. For (A) and (B) the n is shown in each column. Data are shown as mean ± SE. p values are shown in the panels and were obtained by ANOVA with Tukey's correction. For panel (A) each mutant was compared with WT by ANOVA with Tukey's correction and the rescue was compared with *kcc-1* by t-test.

behavioral phenotype, they displayed distinct Ca^{2+} phenotypes in ASH neurons. More specifically, Ca^{2+} transients were larger than wild type and did not adapt in *kqt-2* mutants (Figures 4B and S5C). In *egl-36* and *kcc-1* mutants they did not adapt but were not statistically different in amplitude than wild type (Figures 4D,4G and S5C). In *egl-36* mutants Ca^{2+} transients were also faster than wild type (Figure 4L). Finally, in *best-9* mutants Ca^{2+} transients were statistically slower than in wild type, but their amplitude was similar to wild type (Figures 4J,4L and S5C). *ent-4* is the only mutant that displayed Ca^{2+} transients that were just like wild type (Figure 4F). One possibility is that in this mutant, secondary octanol sensing neurons ADL or AWB might be affected. We note that in *kcc-1*mutant, the second exposure to octanol leads to Ca^{2+} transients that are actually larger than the ones caused by exposure to the odorant the first time (Figure 4G). We hypothesized that this might be because of dysregulation of both K^+ and Cl^- ions in this mutant perhaps leading to depletion of GABA in Amsh glia or no Cl^- available for the $GABA_A$ receptor LGC-38 in the ASH, like we have shown in *clh-1*mutant.[24] To test this idea, we cultivated *kcc-1* mutants on plates containing 150 mM KCl, in an attempt to restore KCl balance. We found that in these conditions the second Ca^{2+} transient is now smaller than the first (Figures S6L-S6O). Of interest, *kcc-1* mutants reared on high KCl displayed a partially rescued behavioral phenotype, supporting that Ca^{2+} transients adaptation plays a key role in behavior, as we have demonstrated for nose touch responses (Figure S6P).[24]

To determine whether these ASH Ca^{2+} phenotypes were caused by loss of these genes in Amsh glia, we performed rescue experiments in mutant animals expressing wild type cDNA for the corresponding gene in Amsh glia. We found that the Ca^{2+} phenotypes were rescued, supporting that it is loss of these genes in Amsh glia, and not their global knockout, that causes the neuronal phenotypes (Figures 4C, 4E, 4H, 4I, 4K, and 4L). We conclude that *kqt-2*, *egl-36*, *kcc-1*, and *best-9* function in Amsh glia to regulate the response of ASH neurons to octanol (Figure 8).

We published that knockout of Amsh glial channel *clh-1* causes elevated basal Ca^{2+} in ASH neurons which correlates with reduced nose touch avoidance response.[24] We thus wondered whether basal Ca^{2+} was elevated in *kqt-2*, *egl-36*, *kcc-1*, *best-9*, or *ent-4* mutants. Thus, we measured basal GCaMP-6s fluorescence in ASH of wild type and mutants. We found that only *kcc-1* displayed changes in basal Ca^{2+} as compared to wild type, but contrary to *clh-1* mutants, basal Ca^{2+} was reduced in *kcc-1*, nevertheless suggesting altered basal excitability in this mutant (Figure 5A).[24] To confirm that reduced basal Ca^{2+} in *kcc-1* was because of loss of *kcc-1* in Amsh glia, we repeated the experiments in human KCC1 and worm KCC-1 glia rescue animals and observed that in these animals basal Ca^{2+} in ASH was just like in wild type (Figure 5A). Again, the use of human KCC1 for the rescue experiments supports conservation of function of this K^+/Cl^- cotransporter across species.

Because *kcc-1* mutants have reduced basal Ca^{2+} levels in ASH as compared to wild type (Figure 5A), we next asked whether this stemmed from excessive tonic GABA signaling. Indeed, we have published that Amsh glia tonically release GABA, which keeps the concentration of basal Ca^{2+} in ASH in check, preventing hyperexcitability.[24] Thus, we quantified the basal Ca^{2+} level in ASH of *kcc-1* mutants treated with the $GABA_A$ antagonist bicuculline, and we found that it was higher than in *kcc-1* mutants and close to wild type levels (Figure 5B), supporting our hypothesis. As previously shown, the Ca^{2+} levels of wild type ASH are also increased by treatment with bicuculline.[24] To summarize, loss of *kqt-2*, *egl-36*, *kcc-1*, and *best-9* in glia leads to distinct effects on ASH excitability, which in the case of *kcc-1* may involve increase in GABA signaling at baseline which could result in GABA depletion during stimulation with odorants (see Figure 4G).

Duan et al. showed that disruption of GABA-mediated glia/neuron crosstalk in the Amphid sensory organ leads to reduced ASH neuron and behavioral adaptation to octanol.[23] Our Ca^{2+} imaging experiments show

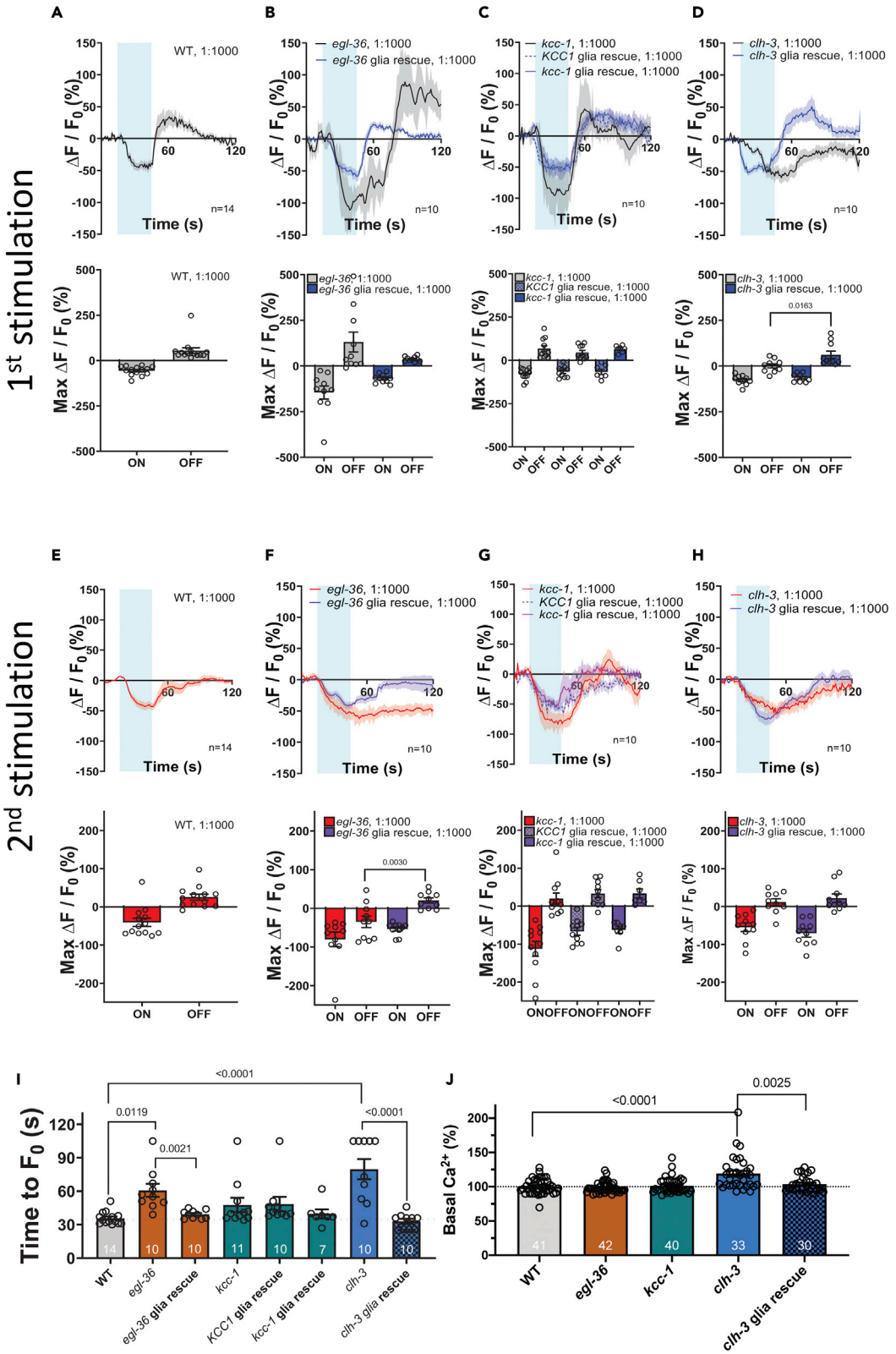
A
B
C
D
1st stimulation
WT, 1:1000
egl-36, 1:1000
egl-36 glia rescue, 1:1000
kcc-1, 1:1000
KCC1 glia rescue, 1:1000
kcc-1 glia rescue, 1:1000
clh-3, 1:1000
clh-3 glia rescue, 1:1000
ΔF / F0 (%)
Time (s)
n=14
n=10
Max ΔF / F0 (%)
ON
OFF
0.0163
E
F
G
H
2nd stimulation
0.0030
I
J
Time to F0 (s)
Basal Ca2+ (%)
<0.0001
0.0119
0.0021
0.0025
WT
egl-36
egl-36 glia rescue
kcc-1
KCC1 glia rescue
kcc-1 glia rescue
clh-3
clh-3 glia rescue

Figure 6. AWC neuronal activity in response to diluted isoamyl alcohol in channel and transporter mutants

(A) Calcium transients generated in AWC neurons by perfusion with isoamyl alcohol (1:1,000, cyan shaded area) as measured by % increase of GCaMP5 fluorescence above the baseline ($\Delta F/F_0$) in wild type and *egl-36*, *egl-36* glia rescue worms, *kcc-1*, human KCC1 glia rescue strain, worm *kcc-1* glia rescue worms, *clh-3*, and *clh-3* glia rescue worms for the first stimulation (A-D) and the second stimulation (E-H). The bar graphs show the peak percentage of GCaMP-6s ($\Delta F/F_0$upon odorant perfusion (ON) and odorant removal (OFF). The number of neurons tested is shown in the graphs.

(I) Time it takes for the fluorescence to return to F_0 after odorant removal during the first exposure to isoamyl alcohol for wild type, mutants, and related glia specific rescue strains.

(J) The relative to wild type basal calcium in AWC neurons of the indicated strains which have reduced attraction to isoamyl alcohol and their rescue strains: *egl-36*, *egl-36* glia rescue, *kcc-1*, *clh-3*, and *clh-3* glia rescue. N is indicated in each column. Data are shown as mean ± SE. p values are shown in the panels and were obtained by unpaired Student's t-test or in the case of panels I and J, by ANOVA with Tukey's correction, comparing each mutant with WT. Rescues were compared with the corresponding mutant by t-test.

that ASH neuronal adaptation to the second exposure to octanol is lost in *kqt-2*, *egl-36*, and *kcc-1* (Figures 4B, 4D and 4G). We thus wondered whether these mutants also displayed reduced behavioral adaptation to this odorant. Therefore, we assayed adaptation in behavioral experiments, using *unc-25* Amsh glia RNAi as negative control. *unc-25* encodes for the GABA synthetic enzyme glutamate decarboxylase (GAD).[44] We found that *kqt-2*, *egl-36*, and *kcc-1* mutants displayed reduced adaptation as compared to wild type, suggesting positive correlation between ASH neuron and behavioral adaptation in these mutants (Figure 5C). However, although *best-9* and *ent-4* mutants also showed reduced adaptation to octanol in behavioral experiments, their ASH Ca^{2+} transients still displayed robust adaptation to octanol. These results suggest that behavioral adaptation to octanol is more complex than previously thought,[23] and may involve other cells/mechanisms. For example, we note that Amsh glia Ca^{2+} transients are greatly reduced in both *best-9* and *ent-4* mutants and their basal Ca^{2+} level is elevated as compared to wild type suggesting a glial "adapted" state in these mutants. These data suggest a more direct link than previously suspected between glial physiology and behavior.

Ca^{2+} transients in AWC neurons are altered by loss of glial channels and transporters

AWC neurons are a pair of chemosensory neurons whose fan-like cilia are embedded in the Amsh glia (Figure 2H). *C. elegans* responds to low concentrations of the odorant isoamyl alcohol via AWC neurons.[28] Low concentrations of isoamyl alcohol are attractive to the worm. At higher concentrations though, isoamyl alcohol is repulsive to *C. elegans* and it is sensed not only by AWC, but also by ASH and AWB neurons.[45] Furthermore, high concentrations of this odorant induce intracellular Ca^{2+} transients in the Amsh glial cells.[23] Given that behavior is tested on agar plates but the response of neurons to odorants is tested using a perfusion system in which the odorant is directly perfused onto the nose of the animal, it may be difficult to directly compare results obtained with the two methods. However, previously published work has firmly established that on plates 1:100 isoamyl alcohol is attractive.[29] On the contrary, 1:100 dilution in imaging experiments elicits activation of Amsh glia and is considered repulsive.[23] In behavioral assays using isoamyl alcohol at the concentration of 1:100, *egl-36*, *kcc-1*, and *clh-3* mutants display reduced attraction (Figure 1C). However, these mutants also showed altered Ca^{2+} transients in Amsh glia following perfusion of this odorant at the 1:100 dilution directly on the nose of the animals (Figures 3J-3L). We thus reasoned that loss of these genes in glia might dampen the response of sensory neurons to a wide range of isoamyl alcohol concentrations. For this reason, we recorded Ca^{2+} transients in AWC neurons upon perfusion of isoamyl alcohol at 1:1000 and 1:100 dilutions. Moreover, because Amsh glia mediate adaptation of ASH neurons, we monitored the AWC response to two consecutive exposures to isoamyl alcohol to establish whether adaptation occurs in these neurons and if it is regulated by Amsh glia (Figures 6 and 7).

In wild type animals, perfusion with 1:1000 isoamyl alcohol led to a decrease in intracellular Ca^{2+}, whereas removal of the odorant caused an increase in intracellular Ca^{2+}, as previously reported (Figure 6A).[45–47] These changes in intracellular Ca^{2+} are thought to be because of a reduction in the function of the guanylyl cyclases ODR-1 and DAF-11 upon exposure to isoamyl alcohol, followed by an increase in its function upon odorant removal, which leads to production of cGMP and activation of cGMP-gated cationic channel TAX-2/TAX-4.[48,49] These changes in intracellular Ca^{2+} in AWC neurons mediate *C. elegans* turning toward the source of the odorant.[46,50] In *egl-36* and *kcc-1* mutants, we found similar changes in intracellular Ca^{2+}upon application and removal of isoamyl alcohol (Figures 6B and 6C), though in *egl-36* mutants the rise of Ca^{2+}upon odorant removal was slower (Figure 6I). However, in *clh-3* mutants, the typical rise of intracellular Ca^{2+}upon odorant removal was completely absent (Figures 6D and 6I). Importantly, both in *egl-36* and *clh-3* mutants the expression of wild type cDNA corresponding to these genes in Amsh glia rescued Ca^{2+} transients (blue line, Figures 6B and 6D). These results support that the changes in AWC excitability

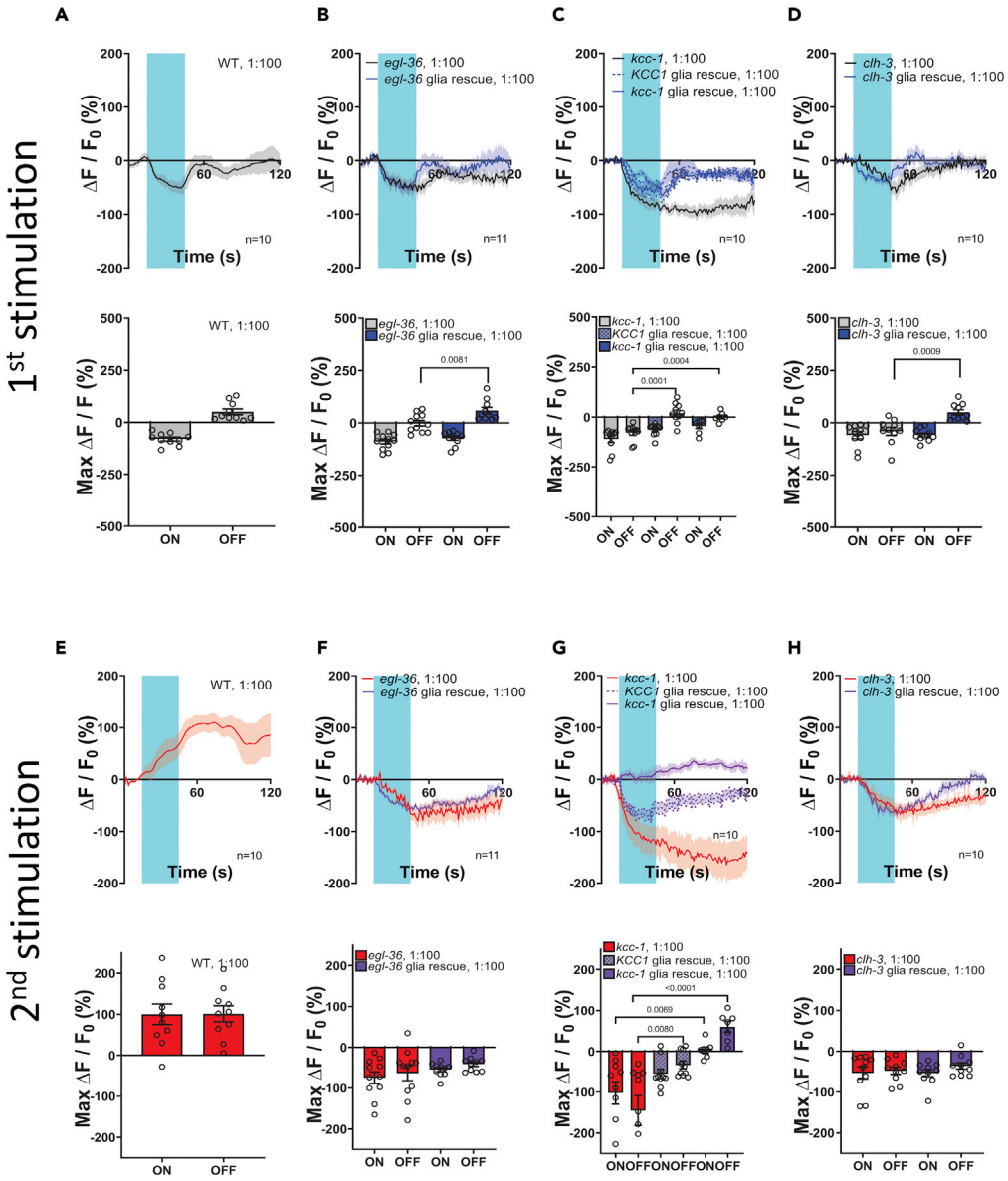

Figure 7. Glial channels and transporters are needed for the function of AWC neurons in response to concentrated isoamyl alcohol

(A) Calcium transients generated in AWC neurons by perfusion with isoamyl alcohol (1:100, cyan shaded area) as measured by % increase of GCaMP5 fluorescence above the baseline ($\Delta F/F_0$) in wild type *egl-36*, *egl-36* glia rescue, *kcc-1*, human KCC1 glia rescue, worm *kcc-1* glia rescue, *clh-3*, and *clh-3* glia rescue for the first stimulation (A–D) and the second stimulation (E–H). The bar graphs show the peak percentage of GCaMP5 ($\Delta F/F_0$) upon odorant perfusion (ON) and odorant removal (OFF). The number of neurons tested is shown in the graphs. Data are shown as mean ± SE. p values are shown in the panels and were obtained by unpaired Student's t-test.

in these mutants are because of loss of *egl-36* and *clh-3* in Amsh glia. This is somewhat surprising because Duan et al. showed that 1:1000 isoamyl alcohol does not activate Amsh and thus suggest that *egl-36* and *clh-3* channels control basal Amsh glial regulation of the function of AWC neurons, independent from glial response to this odorant.[23]

In wild type animals, second exposure to 1:1000 isoamyl alcohol led to a similar decrease in intracellular Ca^{2+}, but to a smaller increase upon odorant removal (Figure 6E). This result suggests that AWC adapts to consecutive exposures to isoamyl alcohol. Although *kcc-1* and *clh-3* had responses to a second exposure

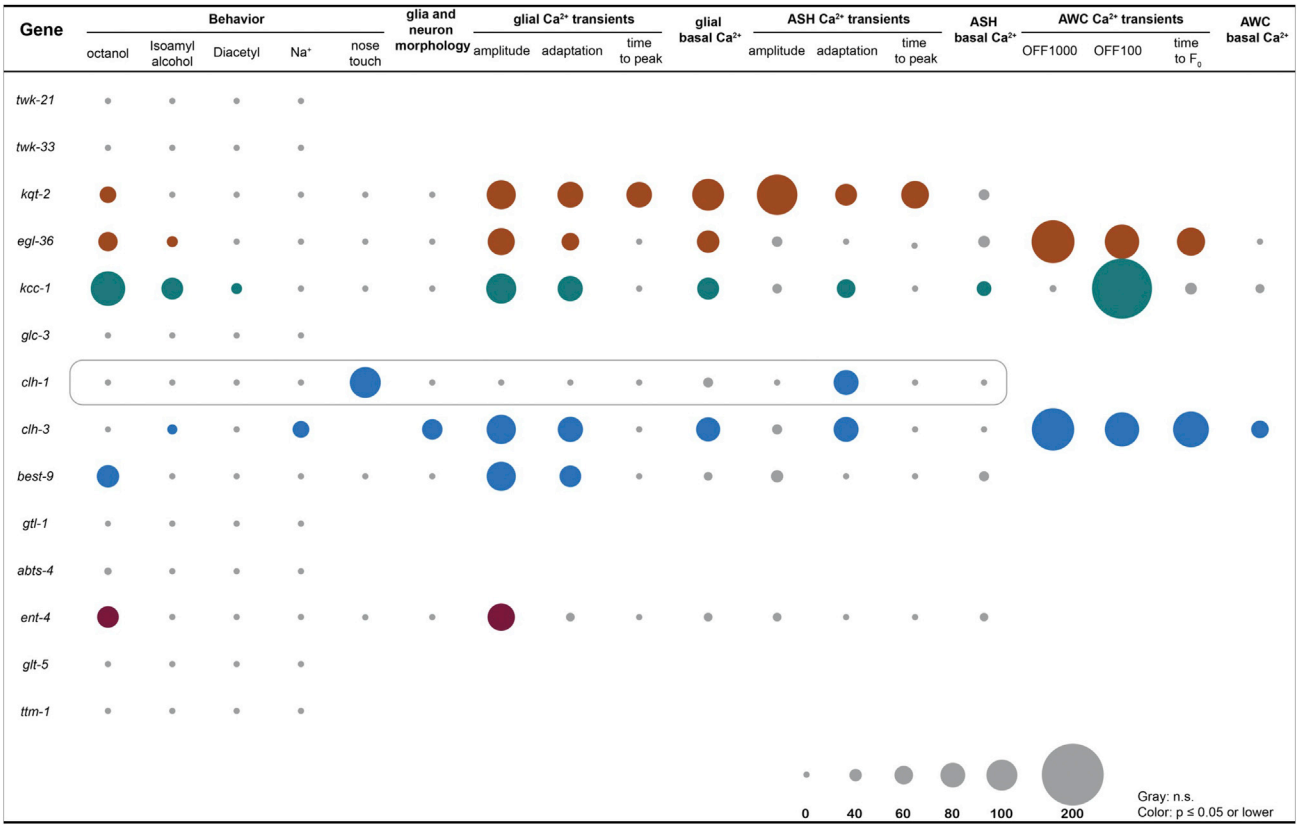

Figure 8. Summary of the behavioral, morphological, and functional phenotypes caused by the loss the glial enriched ion channels and transporters

The size of the dots represents the % of change compared to wild type which was set as 0%. The not significant values are shown in gray. The significant values are shown in color. The colors correspond to the ones used in Figure 1C, thus brown for K^+ channel genes, green for the K^+/Cl^- transporter, blue for the Cl^- channels, and magenta for solute carrier family genes.

to 1:1000 isoamyl alcohol that were like wild type, *egl-36* did not (Figure 6F). In particular, there was no recovery from Ca^{2+} decrease, suggesting that in *egl-36* mutant adaptation to the second exposure of the odorant is stronger. Importantly, this phenotype is rescued by expression of *egl-36* in Amsh, underscoring that it is the loss of *egl-36* in glia rather than AWC neurons that causes the phenotype (purple line, Figure 6F). Rescue in Amsh glia of *kcc-1* (using either human or worm cDNAs) and *clh-3* leads to results identical to the respective mutants and wild type (Figures 6G and 6H). Finally, we quantified basal Ca^{2+} in AWC neurons of wild type and mutants and found that it was higher than in wild type in *clh-3*. Expression of *clh-3* cDNA in Amsh glia of the *clh-3* knockout rescued basal Ca^{2+} to wild type levels (Figure 6J). Taken together, these data show that glial K^+ channel *egl-36* plays a key role in the response of AWC neurons to isoamyl alcohol removal, which is essential to mediate the worms' reorientation toward the source of the odorant.[46,50] In this mutant, this reduced response is seen also upon exposure to this odorant a second time, suggesting that it is because of reduced sensitivity of AWC neurons to isoamyl alcohol (Figures 6F and 6I). The Cl^- channel *clh-3*, on the other hand, is needed for AWC response to isoamyl alcohol removal the first but not the second time, and for basal Ca^{2+} in these neurons, suggesting that glial CLH-3 may be needed for basal AWC excitability.

Surprisingly, in *kcc-1* mutants, AWC neurons respond normally to 1:1000 isoamyl alcohol. What happens when this odorant is perfused at 1:100, a concentration known to activate Amsh glia? In wild type animals, AWC neurons displayed a decrease in intracellular Ca^{2+}upon exposure to the odorant and an increase in intracellular Ca^{2+}upon odorant removal that is smaller than the one observed at the 1:1000 dilution (Figure 7A), which is consistent with published work.[49] Of interest, though, at this concentration of isoamyl alcohol, *kcc-1* mutants showed a phenotype more severe than the one seen in *egl-36* and *clh-3* mutants (Figures 7B–7D). Indeed, in *kcc-1* mutants intracellular Ca^{2+} did not return to control levels after exposure

to 1:100 isoamyl alcohol, whereas in *egl-36* and *clh-3* mutants there was a partial return. In all three mutants, Ca^{2+} transients were rescued to control levels by expression of wild type cDNA (human or worm in the case of *kcc-1*) in Amsh, again supporting the idea that it is the loss of these genes in Amsh that is responsible for the neuronal phenotypes (blue line and columns, Figures 7B–7D). These data support the idea that the function of *kcc-1* might be needed specifically for mediating glia/AWC cross talk at higher concentrations of isoamyl alcohol. Given that *kcc-1* is needed for chemotaxis to isoamyl alcohol on plates, these results suggest the 1:100 dilution in imaging experiments, previously considered repulsive,[45] is likely still in the attractive range for this odorant. This is in line with the fact that Yoshida et al. used GCaMP2 for their imaging experiments, a less sensitive calcium sensor than GCaMP5 which we used here[51]

When we looked at the response of AWC neurons to the second exposure to 1:100 isoamyl alcohol in wild type animals, we observed an interesting phenomenon: application of the odorant causes an increase in Ca^{2+} rather than a decrease. This increase in Ca^{2+} persists for the entire duration of the recording (Figure 7E), but eventually returns to the basal level after ~2 min (Figure S9A). The increase in intracellular Ca^{2+}upon odorant application was not seen in *egl-36*, *kcc-1*, or *clh-3* mutants. Rather, in all three mutants there was a marked reduction of Ca^{2+}upon odorant application, with the reduction being the largest in *kcc-1* mutants (Figures 7F–7H). Expression of human KCC1 in Amsh partially rescued, whereas expression of worm KCC-1 fully rescued Ca^{2+} transients (purple dotted and continuous lines, and checkered and solid bars, respectively, Figure 7G). Of interest, expression of the corresponding wild type cDNA did not restore the wild type response upon exposure to 1:100 isoamyl alcohol a second time in *egl-36* and *clh-3*, suggesting that there might be a neuronal component to this phenotype. Because *kcc-1* encodes for a transporter that extrudes K^+ and Cl^-, we wondered whether it could perform this function from the AWC neuron's plasma membrane rather than from the Amsh glia. We thus expressed worm KCC-1 in the AWC neurons of the *kcc-1* mutant. We found that attraction to isoamyl alcohol and Ca^{2+} transients were partially rescued (Figures S9B-S9F). These results show that KCC-1, even though it is not detected in AWC neurons,[26] could still function by being expressed in these neurons rather than the glia. We conclude that *egl-36*, *kcc-1*, and *clh-3* are all needed in Amsh glia for AWC neuron response to 1:100 concentration of isoamyl alcohol (Figure 8).

DISCUSSION

We show here the first systematic and unbiased, albeit not comprehensive, analysis of the function of glial regulators of ion and solute flux in chemotaxis. Our analysis reveals the importance of glial regulators of K^+, Cl^-, and nucleoside homeostasis, and interesting distinctions between affected sensory neurons.

Amsh glia ablated *C. elegans* display severely reduced response to octanol, isoamyl alcohol, diacetyl, and Na-acetate (Figures S3A-S9D).[16] Yet the knockout of glial enriched genes has considerably different effects on these sensory modalities. Indeed, octanol avoidance is the most affected with the knockout of 5 genes causing delayed response to this odorant, whereas chemotaxis to diacetyl and Na-acetate are the least affected with only *kcc-1* and *clh-3* mutants, respectively, showing reduced attraction (Figure 1C). Although glia ablation is known to disrupt the cilia of AWC and AWA olfactory neurons,[16] phenotypes that we have not observed in the mutants analyzed here (Figures 2E-2L), these differences suggest high specificity of regulation of chemosensory functions by glial genes. One mechanism that could explain this specificity is subcellular localization. This type of mechanism is enacted by the K^+/Cl^- cotransporter KCC-3, which is localized in the Amsh membrane microdomain facing the cilia of AFD thermosensory neurons. In mammals, KCC and NKCC co-transporters are expressed in glia,[52,53] and their disruption can lead to sensory neuropathy.[54] KCC-3 regulates the extracellular concentration of Cl^- around the AFD cilia, leading to regulation of the function of guanylyl cyclase GCY-8 and consequently of the animal's response to temperature.[21] However, possibly because of the spatially restricted expression of KCC-3, this transporter does not influence the response to nose touch mediated by ASH neurons.[24] Thus, other glial regulators of ion and solute flux, not analyzed here, could play a more prominent role in regulating the function of AWA and ASE neurons. Alternatively, AWA and ASE neurons may be less sensitive to the activity of glial regulators of ion and solute flux. Given the proven impact of K^+ and Cl^- ions on the function of neurons, this explanation seems less likely, but because Amsh glia ensheath only the cilia and not the entire neuron, this could still be consistent with function.

Because the plasma membrane is mostly permeable to K^+ at rest, the extracellular concentration of K^+ has a major role in establishing the membrane potential and thus the excitability of neurons. Glia across species have been shown to remove excess extracellular K^+ during high electrical activity.[55,56] However, we have

also shown that glia mediate K^+ excretion, thereby modulating neuronal excitability. Indeed, we have previously published that Na^+ channels of the DEG/ENaC family and the Na^+/K^+ ATPase expressed in glia associated with sensory neurons regulate neuronal output, likely by regulating K^+ excretion in the microenvironment between glia and neurons.[17–19,22] Potassium reuptake and excretion is also known to occur in the sensory sensilla of insects and in the vertebrate inner ear, where the concentration of K^+ is well above the typical extracellular concentration of ~5 mM.[57,58] So it is not surprising that two K^+ channels, *kqt-2* and *egl-36*, were found in this study to be required for octanol avoidance and chemotaxis to isoamyl alcohol. While *kqt-2* is a homolog of KCNQ channels, *egl-36* is a homolog of Kv 3 channels that underlie the "A" type inactivating K^+ current. Both these channels are gated by voltage, are highly expressed in neurons, and have been implicated in epilepsy and other neurological disorders.[59–63] Of interest, though, both KCNQ and Kv 3 channels have been reported to be expressed in glia including astrocytes, oligodendrocytes, and microglia.[64–66] Here KCNQ channels have been suggested to be involved in migration of these cells, whereas Kv 3 channels were proposed to help with the repolarization of the membrane of astrocytes and with the entry of calcium.[65–67] The discovery that these voltage-gated K^+ channels regulate neuronal output in the amphid sensory organ of *C. elegans* adds to our understanding of the function of these channels in glia in other systems and species, and suggests that these glial channels could be considered as targets for the treatment of epilepsy and other neurological disorders.

Recent work showed that there are paracrine signals between Amsh glia and sensory neurons in *C. elegans*, much like between glial cells and neurons in the nervous system of higher organisms.[23,24] Both Duan et al. and our lab have shown that Amsh glia respond cell-autonomously to odorants and touch and consequently release the neurotransmitter GABA. GABA released by the Amsh glia dampens the excitability of the polymodal neurons ASH, mediating adaptation of these neurons to repeated stimulations. We have also shown that glial expressed CLH-1 channel mediates efflux of Cl^- ions from glia.[24] These Cl^- ions then permeate through the $GABA_A$ receptor LGC-38, reducing neuronal excitability and thereby mediating adaptation. Importantly, the CLH-1 mammalian homolog ClC-2 is also expressed in glia, including astrocytes and oligodendrocytes, where it regulates ionic homeostasis and pH.[68,69] Regulation of Cl^- homeostasis by glial ClC-2 might be important for GABA signaling given that ClC-2 is localized in astrocytic endfeet that ensheath capillaries and in the neurophil of the stratum pyramidale in close proximity to GABAergic neurons.[70] In this study, we found that all the mutants displaying reduced response to octanol are also characterized by reduced adaptation (Figure 5C), a sign that these genes might be involved, either directly or indirectly, in regulating GABA signaling. Intriguingly, three of these genes are mediators of Cl^- homeostasis, the CLH-1 homolog CLH-3, the bestrophin channel BEST-9, and the K^+/Cl^- cotransporter KCC-1, a close homolog of KCC-3. In particular, KCC-1 mediates transport of K^+ and Cl^- ions outside the cell and thus it is expected to cause either the removal or the accumulation of Cl^- in the microenvironment between glia and neurons, depending on whether the transporter is expressed on the apical (cilia facing) or basolateral membrane of the Amsh glia, respectively. Our basal intracellular Ca^{2+} analysis in ASH neurons plus and minus bicuculline suggests that KCC-1 is expressed on the basolateral membrane. Indeed, ASH neurons of *kcc-1* mutants have lower basal intracellular calcium than wild type, suggesting membrane hyperpolarization and therefore stronger GABA inhibition at baseline. This idea is supported by the fact that bicuculline rescues this phenotype (Figure 5B). Future immune electron microscopy studies will test this hypothesis directly. Of interest, in *kcc-1* ASH neurons do not adapt upon repeated stimulations, suggesting that although tonic GABA may be elevated in these mutants, phasic GABA release upon repeated stimulations with octanol is reduced (Figure 4F). This is different than what we found in *clh-1* mutants where both tonic and phasic GABA signaling were reduced, and thus suggests that different Cl^- imbalances lead to distinct phenotypes, perhaps as a result of different effects on the membrane potential. A mechanism involving BEST-9 is more difficult to hypothesize, but the slower Ca^{2+} transients in ASH neurons of *best-9* mutants suggest slower recruitment of Ca^{2+} permeable channels upon stimulation with octanol. Given that bestrophins are highly permeable to bicarbonate,[71] this could be an effect of pH, perhaps specifically on the octanol receptor of ASH neurons or on Ca^{2+} permeable OSM-9 and EGL-19 channels.[23]

We report here also for the first time an analysis of AWC neuronal response to repeated exposures to diluted and concentrated isoamyl alcohol, and the effect of knockout of glial enriched channel and transporter genes on their activity. AWC are odorant-OFF neurons which means they are activated by odorant removal.[45–47] Thus, mutations that alter the OFF response of AWC neurons are expected to reduce chemotaxis to isoamyl alcohol. Our data support this idea with knockout of *egl-36*, *kcc-1*, and *clh-3* all altering the

OFF response and causing reduced attraction to isoamyl alcohol (Figures 1, 6 and 7). Moreover, our data show that AWC neurons undergo adaptation. Future studies will establish whether this phenomenon is cell autonomous or whether it is mediated by neuromodulators released by Amsh glia or both. However, the involvement of GABA in AWC adaptation seems unlikely based on results of ASH/AWC cross-adaptation and optogenetic experiments reported by Duan et al.[23] If not via GABA or neuromodulator signaling, how might K^+ channel *egl-36*, K^+/Cl^- cotransporter *kcc-1*, and Cl^- channel *clh-3* regulate the response and adaptation of AWC neurons to isoamyl alcohol? Although K^+ may be needed to set the excitability of AWC sensory neurons, as described above, Cl^- might be needed in the Amph sensory organ to accompany K^+ movement and allow water transport. Future more mechanistic studies will distinguish between these possibilities.

One of the genes identified in our small-scale screen of glial enriched genes required for octanol avoidance is the equilibrative nucleoside transporter ENT-4 (Figure 1C). Intriguingly, it is the only gene whose knockout does not alter basal Ca^{2+} in Amsh glia, consistent with the idea that it is not a mediator of ion flux (Figure 5A). Equilibrative nucleoside transporters transport naturally occurring purines including adenosine, guanosine, and inosine, and pyrimidines such as uridine, cytidine, and thymidine, all of which are metabolic precursors for DNA, RNA, and ATP. However, these nucleosides also serve as signaling molecules and neuromodulators.[72] For example, adenosine binds to adenosine receptors, and in the nervous system it modulates neurotransmitter release and synaptic plasticity.[73–75] It is noteworthy that mammalian ENT-4 (also called PMAT) also mediates the low affinity transport of dopamine and serotonin, raising the possibility that Amsh glia ENT-4 might be involved in clearing of neurotransmitters.[76]

Finally, one unexpected finding of our analysis is that there are several glial enriched ion channels and transporters that seem to have little relevance for basic chemotaxis function. For example, we did not observe any phenotype in mutants of the glutamate transporter *glt-1* or in strains in which the two-pore domain K+ channels *twk-21* and *twk-33* had been knocked down in glia, despite these being amongst the most enriched genes in Amsh glia (Figures 1A–1C). Because we have not analyzed other sensory phenotypes, we think that this once again points to the possibility that different neurons may have different requirements and sensitivity to perturbations in their microenvironment.

Taken together, our findings provide evidence that K^+ channels of the KCNQ and Kv3 families, Cl^- channels of the ClC and bestrophin families, K^+/Cl^- co-transporters, and equilibrative nucleoside transporters are all needed in an accessory cell of a sensory organ for chemosensory responses. This work lays the foundation for future investigations of the mechanisms underlying regulation of sensory functions by accessory cells, and for a better understanding of how sensory signals are processed and integrated at the periphery.

Limitations of the study

This is the first systematic unbiased small screen of glial regulators of the concentration of ions and solutes in chemosensory function in *C. elegans*. Our work identifies players in the cross talk between accessory and sensory cells in the Amphid organ of the worm that may be conserved across species and across different parts of the nervous system. However, one of the limitations of this study is that it is not comprehensive. Indeed, not all genes and not all the sensory modalities carried out by the Amphid sensory organ were investigated. For example, there are several innexin genes enriched in Amsh glia and many more are expressed in these cells (Figure S2). Innexins are homologs of mammalian Pannexins and function both as gap junctions and plasma membrane channels.[77–79] Because Amsh glia do not appear to be connected to any other cell via gap junctions,[80] innexins in these cells likely function as plasma membrane channels involved in the control of the membrane potential or the release of neuromodulators.[77,78]

In addition, Figure S2 shows many more channels and transporters that are detected in Amph glia by RNA sequencing, all of which are bound to have a function in glial physiology and could potentially be implicated in glia/neuron cross talk. These channels and transporters are not enriched in Amsh glia though, thus they may be implicated in functions that are shared with other cell types. Finally, other sensory modalities including response to temperature, UV light, sound, and electric fields were not investigated here and could be altered in some of the mutants we studied.[30–34]

Another limitation of this study is that it does not definitively identify the molecular mechanisms underlying the regulation of sensory function by the investigated channels and transporters. Our results point to both GABA-dependent and independent mechanisms potentially involving other neuromodulators. Future studies in which the subcellular localization of these channels and transporters will be determined by immunoelectron microscopy and in which intracellular pathways and various neurotransmitters will be probed, will establish these molecular mechanisms. All these studies require optimization and are beyond the scope of this manuscript. Our study though provides additional insights on the functional cross talk between the Amsh glia and sensory neurons in *C. elegans* and provides several leads for future studies.

STAR★METHODS

Detailed methods are provided in the online version of this paper and include the following:

- KEY RESOURCES TABLE
- RESOURCE AVAILABILITY
  - Lead contact
  - Materials availability
  - Data and code availability
- EXPERIMENTAL MODEL AND SUBJECT DETAILS
  - C. elegans
- METHODS DETAILS
  - Molecular biology
  - Comparison of gene-expression
  - Behavioral assays
  - Fluorescence and confocal microscopy
  - Calcium imaging
  - Chloride imaging
- QUANTIFICATION AND STATISTICAL ANALYSIS

SUPPLEMENTAL INFORMATION

Supplemental information can be found online at https://doi.org/10.1016/j.isci.2022.105684.

ACKNOWLEDGMENTS

We thank Yuji Kohara, Atsushi Kuhara, and William R. Schafer for sharing DNA plasmids. We thank the Caenorhabditis Genetic Center (USA) and National BioResource Project (NBRP, Japan) for strains. We thank Stephen Roper, Rong Grace Zhai, Robert W. Keane, Peter H. Larsson, and Kevin Collins, for sharing equipment essential for data collection. Finally, we thank Joel Hernandez Barreto for help with some of the behavioral assays. This work was supported by NIH Grants R01s NS070969 and NS105616A1.

AUTHOR CONTRIBUTIONS

L.W. designed and performed experiments, analyzed data, drafted, and edited the manuscript, B.G. designed and performed experiments, analyzed data, and edited the manuscript, N.E, performed experiments and analyzed data, J.F.A. designed and performed experiments, analyzed data, and edited the manuscript, D.H.K., performed experiments, L.B. managed the project, designed experiments, analyzed data, wrote the manuscript.

DECLARATION OF INTERESTS

All authors declare no competing interests.

INCLUSION AND DIVERSITY

We support inclusive, diverse, and equitable conduct of research.

Received: March 30, 2022
Revised: September 11, 2022
Accepted: November 24, 2022
Published: December 22, 2022

REFERENCES

1. Breipohl, W., Laugwitz, H.J., and Bornfeld, N. (1974). Topological relations between the dendrites of olfactory sensory cells and sustentacular cells in different vertebrates. An ultrastructural study. J. Anat. *117*, 89–94.

2. Rafols, J.A., and Getchell, T.V. (1983). Morphological relations between the receptor neurons, sustentacular cells and Schwann cells in the olfactory mucosa of the salamander. Anat. Rec. *206*, 87–101. https://doi.org/10.1002/ar.1092060111.

3. Getchell, T.V. (1986). Functional-properties of vertebrate olfactory receptor neurons. Physiol. Rev. *66*, 772–818.

4. Doty, R.L. (1995). Handbook of olfaction and gustation (Vol 32, Pg 1432, 1995). Neurology *45*, 1952.

5. Platt, N., Suzuki, H., Kurihara, Y., Kodama, T., and Gordon, S. (1996). Role for the class A macrophage scavenger receptor in the phagocytosis of apoptotic thymocytes in vitro. Proc. Natl. Acad. Sci. USA *93*, 12456–12460. https://doi.org/10.1073/pnas.93.22.12456.

6. Bartel, D.L., Sullivan, S.L., Lavoie, E.G., Sévigny, J., and Finger, T.E. (2006). Nucleoside triphosphate diphosphohydrolase-2 is the ecto-ATPase of type I cells in taste buds. J. Comp. Neurol. *497*, 1–12. https://doi.org/10.1002/cne.20954.

7. Vandenbeuch, A., Anderson, C.B., Parnes, J., Enjyoji, K., Robson, S.C., Finger, T.E., and Kinnamon, S.C. (2013). Role of the ectonucleotidase NTPDase2 in taste bud function. Proc. Natl. Acad. Sci. USA *110*, 14789–14794. https://doi.org/10.1073/pnas.1309468110.

8. Dvoryanchikov, G., Sinclair, M.S., Perea-Martinez, I., Wang, T., and Chaudhari, N. (2009). Inward rectifier channel, ROMK, is localized to the apical tips of glial-like cells in mouse taste buds. J. Comp. Neurol. *517*, 1–14. https://doi.org/10.1002/cne.22152.

9. Cherkashin, A.P., Kolesnikova, A.S., Tarasov, M.V., Romanov, R.A., Rogachevskaja, O.A., Bystrova, M.F., and Kolesnikov, S.S. (2016). Expression of calcium-activated chloride channels Ano1 and Ano2 in mouse taste cells. Pflugers Arch. *468*, 305–319. https://doi.org/10.1007/s00424-015-1751-z.

10. Guarascio, D.M., Gonzalez-Velandia, K.Y., Hernandez-Clavijo, A., Menini, A., and Pifferi, S. (2021). Functional expression of TMEM16A in taste bud cells. J. Physiol. *599*, 3697–3714. https://doi.org/10.1113/JP281645.

11. Rodriguez, Y.A., Roebber, J.K., Dvoryanchikov, G., Makhoul, V., Roper, S.D., and Chaudhari, N. (2021). Tripartite synapses" in taste buds: a role for type I glial-like taste cells. J. Neurosci. *41*, 9860–9871. https://doi.org/10.1523/JNEUROSCI.1444-21.2021.

12. Marchese-Ragona, R., Restivo, D.A., De Corso, E., Vianello, A., Nicolai, P., and Ottaviano, G. (2020). Loss of smell in COVID-19 patients: a critical review with emphasis on the use of olfactory tests. Acta Otorhinolaryngol. Ital. *40*, 241–247. https://doi.org/10.14639/0392-100X-N0862.

13. Bryche, B., St Albin, A., Murri, S., Lacôte, S., Pulido, C., Ar Gouilh, M., Lesellier, S., Servat, A., Wasniewski, M., Picard-Meyer, E., et al. (2020). Massive transient damage of the olfactory epithelium associated with infection of sustentacular cells by SARS-CoV-2 in golden Syrian hamsters. Brain Behav. Immun. *89*, 579–586. https://doi.org/10.1016/j.bbi.2020.06.032.

14. Cooper, K.W., Brann, D.H., Farruggia, M.C., Bhutani, S., Pellegrino, R., Tsukahara, T., Weinreb, C., Joseph, P.V., Larson, E.D., Parma, V., et al. (2020). COVID-19 and the chemical senses: supporting players take center stage. Neuron *107*, 219–233. https://doi.org/10.1016/j.neuron.2020.06.032.

15. Zhang, A.J., Lee, A.C., Chu, H., Chan, J.F., Fan, Z., Li, C., Liu, F., Chen, Y., Yuan, S., Poon, V.K., et al. (2021). Severe acute respiratory syndrome coronavirus 2 infects and damages the mature and immature olfactory sensory neurons of hamsters. Clin. Infect. Dis. *73*, e503–e512. https://doi.org/10.1093/cid/ciaa995.

16. Bacaj, T., Tevlin, M., Lu, Y., and Shaham, S. (2008). Glia are essential for sensory organ function in C. elegans. Science *322*, 744–747. https://doi.org/10.1126/science.1163074.

17. Wang, Y., Apicella, A., Jr., Lee, S.K., Ezcurra, M., Slone, R.D., Goldmit, M., Schafer, W.R., Shaham, S., Driscoll, M., and Bianchi, L. (2008). A glial DEG/ENaC channel functions with neuronal channel DEG-1 to mediate specific sensory functions in C. elegans. EMBO J. *27*, 2388–2399. https://doi.org/10.1038/emboj.2008.161.

18. Wang, Y., D'Urso, G., and Bianchi, L. (2012). Knockout of glial channel ACD-1 exacerbates sensory deficits in a C. elegans mutant by regulating calcium levels of sensory neurons. J. Neurophysiol. *107*, 148–158. https://doi.org/10.1152/jn.00299.2011.

19. Han, L., Wang, Y., Sangaletti, R., D'Urso, G., Lu, Y., Shaham, S., and Bianchi, L. (2013). Two novel DEG/ENaC channel subunits expressed in glia are needed for nose-touch sensitivity in Caenorhabditis elegans. J. Neurosci. *33*, 936–949. https://doi.org/10.1523/JNEUROSCI.2749-12.2013.

20. Grant, J., Matthewman, C., and Bianchi, L. (2015). A novel mechanism of pH buffering in C. elegans glia: bicarbonate transport via the voltage-gated ClC Cl- channel clh-1. J. Neurosci. *35*, 16377–16397. https://doi.org/10.1523/JNEUROSCI.3237-15.2015.

21. Singhvi, A., Liu, B., Friedman, C.J., Fong, J., Lu, Y., Huang, X.Y., and Shaham, S. (2016). A glial K/Cl transporter controls neuronal receptive ending shape by chloride inhibition of an rGC. Cell *165*, 936–948. https://doi.org/10.1016/j.cell.2016.03.026.

22. Johnson, C.K., Fernandez-Abascal, J., Wang, Y., Wang, L., and Bianchi, L. (2020). The Na(+)-K(+)-ATPase is needed in glia of touch receptors for responses to touch in C. elegans. J. Neurophysiol. *123*, 2064–2074. https://doi.org/10.1152/jn.00636.2019.

23. Duan, D., Zhang, H., Yue, X., Fan, Y., Xue, Y., Shao, J., Ding, G., Chen, D., Li, S., Cheng, H., et al. (2020). Sensory glia detect repulsive odorants and drive olfactory adaptation. Neuron *108*, 707–721.e8. https://doi.org/10.1016/j.neuron.2020.08.026.

24. Fernandez-Abascal, J., Johnson, C.K., Graziano, B., Wang, L., Encalada, N., and Bianchi, L. (2022). A glial ClC Cl(-) channel mediates nose touch responses in C. elegans. Neuron *110*, 470–485.e7. https://doi.org/10.1016/j.neuron.2021.11.010.

25. Wallace, S.W., Singhvi, A., Liang, Y., Lu, Y., and Shaham, S. (2016). PROS-1/Prospero is a major regulator of the glia-specific secretome controlling sensory-neuron shape and function in C. elegans. Cell Rep. *15*, 550–562. https://doi.org/10.1016/j.celrep.2016.03.051.

26. Taylor, S.R., Santpere, G., Weinreb, A., Barrett, A., Reilly, M.B., Xu, C., Varol, E., Oikonomou, P., Glenwinkel, L., McWhirter, R., et al. (2021). Molecular topography of an entire nervous system. Cell *184*, 4329–4347.e23. https://doi.org/10.1016/j.cell.2021.06.023.

27. Bargmann, C.I., Thomas, J.H., and Horvitz, H.R. (1990). Chemosensory cell function in the behavior and development of Caenorhabditis elegans. Cold Spring Harb. Symp. Quant. Biol. *55*, 529–538.

28. Bargmann, C.I., and Horvitz, H.R. (1991). Chemosensory neurons with overlapping functions direct chemotaxis to multiple chemicals in C. elegans. Neuron *7*, 729–742.

29. Bargmann, C.I., Hartwieg, E., and Horvitz, H.R. (1993). Odorant-selective genes and neurons mediate olfaction in C. elegans. Cell *74*, 515–527.

30. Mori, I., and Ohshima, Y. (1995). Neural regulation of thermotaxis in Caenorhabditis elegans. Nature *376*, 344–348. https://doi.org/10.1038/376344a0.

31. Gabel, C.V., Gabel, H., Pavlichin, D., Kao, A., Clark, D.A., and Samuel, A.D.T. (2007). Neural circuits mediate electrosensory behavior in Caenorhabditis elegans. J. Neurosci. *27*, 7586–7596. https://doi.org/10.1523/JNEUROSCI.0775-07.2007.

32. Edwards, S.L., Charlie, N.K., Milfort, M.C., Brown, B.S., Gravlin, C.N., Knecht, J.E., and Miller, K.G. (2008). A novel molecular solution for ultraviolet light detection in Caenorhabditis elegans. PLoS Biol. *6*, e198. https://doi.org/10.1371/journal.pbio.0060198.

33. Rezai, P., Siddiqui, A., Selvaganapathy, P.R., and Gupta, B.P. (2010). Electrotaxis of Caenorhabditis elegans in a microfluidic environment. Lab Chip *10*, 220–226. https://doi.org/10.1039/b917486a.

34. Iliff, A.J., Wang, C., Ronan, E.A., Hake, A.E., Guo, Y., Li, X., Zhang, X., Zheng, M., Liu, J., Grosh, K., et al. (2021). The nematode C. elegans senses airborne sound. Neuron *109*, 3633–3646.e7. https://doi.org/10.1016/j.neuron.2021.08.035.

35. Coburn, C.M., and Bargmann, C.I. (1996). A putative cyclic nucleotide-gated channel is required for sensory development and function in C. elegans. Neuron *17*, 695–706. https://doi.org/10.1016/s0896-6273(00)80201-9.

36. Komatsu, H., Mori, I., Rhee, J.S., Akaike, N., and Ohshima, Y. (1996). Mutations in a cyclic nucleotide-gated channel lead to abnormal thermosensation and chemosensation in C. elegans. Neuron *17*, 707–718. https://doi.org/10.1016/s0896-6273(00)80202-0.

37. Kindt, K.S., Viswanath, V., Macpherson, L., Quast, K., Hu, H., Patapoutian, A., and Schafer, W.R. (2007). Caenorhabditis elegans TRPA-1 functions in mechanosensation. Nat. Neurosci. *10*, 568–577. https://doi.org/10.1038/nn1886.

38. Wojtyniak, M., Brear, A.G., O'Halloran, D.M., and Sengupta, P. (2013). Cell- and subunit-specific mechanisms of CNG channel ciliary trafficking and localization in C. elegans. J. Cell Sci. *126*, 4381–4395. https://doi.org/10.1242/jcs.127274.

39. Sengupta, P., Chou, J.H., and Bargmann, C.I. (1996). odr-10 encodes a seven transmembrane domain olfactory receptor required for responses to the odorant diacetyl. Cell *84*, 899–909. https://doi.org/10.1016/s0092-8674(00)81068-5.

40. Chen, D., Cheng, H., Liu, S., Al-Sheikh, U., Fan, Y., Duan, D., Zou, W., Zhu, L., and Kang, L. (2022). The voltage-gated calcium channel egl-19 acts on glia to drive olfactory adaptation. Front. Mol. Neurosci. *15*, 907064. https://doi.org/10.3389/fnmol.2022.907064.

41. Boswell-Casteel, R.C., and Hays, F.A. (2017). Equilibrative nucleoside transporters-A review. Nucleosides Nucleotides Nucleic Acids *36*, 7–30. https://doi.org/10.1080/15257770.2016.1210805.

42. Troemel, E.R., Chou, J.H., Dwyer, N.D., Colbert, H.A., and Bargmann, C.I. (1995). Divergent seven transmembrane receptors are candidate chemosensory receptors in C. elegans. Cell *83*, 207–218.

43. Chao, M.Y., Komatsu, H., Fukuto, H.S., Dionne, H.M., and Hart, A.C. (2004). Feeding status and serotonin rapidly and reversibly modulate a Caenorhabditis elegans chemosensory circuit. Proc. Natl. Acad. Sci. USA *101*, 15512–15517. https://doi.org/10.1073/pnas.0403369101.

44. McIntire, S.L., Jorgensen, E., and Horvitz, H.R. (1993). Genes required for GABA function in Caenorhabditis elegans. Nature *364*, 334–337. https://doi.org/10.1038/364334a0.

45. Yoshida, K., Hirotsu, T., Tagawa, T., Oda, S., Wakabayashi, T., Iino, Y., and Ishihara, T. (2012). Odour concentration-dependent olfactory preference change in C. elegans. Nat. Commun. *3*, 739. https://doi.org/10.1038/ncomms1750.

46. Chalasani, S.H., Chronis, N., Tsunozaki, M., Gray, J.M., Ramot, D., Goodman, M.B., and Bargmann, C.I. (2007). Dissecting a circuit for olfactory behaviour in Caenorhabditis elegans. Nature *450*, 63–70. https://doi.org/10.1038/nature06292.

47. Tsunozaki, M., Chalasani, S.H., and Bargmann, C.I. (2008). A behavioral switch: cGMP and PKC signaling in olfactory neurons reverses odor preference in C. elegans. Neuron *59*, 959–971. https://doi.org/10.1016/j.neuron.2008.07.038.

48. L'Etoile, N.D., and Bargmann, C.I. (2000). Olfaction and odor discrimination are mediated by the C. elegans guanylyl cyclase ODR-1. Neuron *25*, 575–586. https://doi.org/10.1016/s0896-6273(00)81061-2.

49. Cheng, H., Liu, Y., Xue, Y., Shao, J., Tan, Z., Liu, S., Duan, S., and Kang, L. (2021). Molecular strategies for intensity-dependent olfactory processing in Caenorhabditis elegans. Front. Mol. Neurosci. *14*, 748214. https://doi.org/10.3389/fnmol.2021.748214.

50. Gray, J.M., Hill, J.J., and Bargmann, C.I. (2005). A circuit for navigation in Caenorhabditis elegans. Proc. Natl. Acad. Sci. USA *102*, 3184–3191. https://doi.org/10.1073/pnas.0409009101.

51. Akerboom, J., Carreras Calderón, N., Tian, L., Wabnig, S., Prigge, M., Tolö, J., Gordus, A., Orger, M.B., Severi, K.E., Macklin, J.J., et al. (2013). Genetically encoded calcium indicators for multi-color neural activity imaging and combination with optogenetics. Front. Mol. Neurosci. *6*, 2. https://doi.org/10.3389/fnmol.2013.00002.

52. Boettger, T., Hübner, C.A., Maier, H., Rust, M.B., Beck, F.X., and Jentsch, T.J. (2002). Deafness and renal tubular acidosis in mice lacking the K-Cl co-transporter Kcc4. Nature *416*, 874–878. https://doi.org/10.1038/416874a.

53. Kettenmann, H., and Verkhratsky, A. (2008). Neuroglia: the 150 years after. Trends Neurosci. *31*, 653–659. https://doi.org/10.1016/j.tins.2008.09.003.

54. Kahle, K.T., Khanna, A.R., Alper, S.L., Adragna, N.C., Lauf, P.K., Sun, D., and Delpire, E. (2015). K-Cl cotransporters, cell volume homeostasis, and neurological disease. Trends Mol. Med. *21*, 513–523. https://doi.org/10.1016/j.molmed.2015.05.008.

55. Kofuji, P., and Newman, E.A. (2004). Potassium buffering in the central nervous system. Neuroscience *129*, 1045–1056. https://doi.org/10.1016/j.neuroscience.2004.06.008.

56. McNeill, J., Rudyk, C., Hildebrand, M.E., and Salmaso, N. (2021). Ion channels and electrophysiological properties of astrocytes: implications for emergent stimulation technologies. Front. Cell. Neurosci. *15*, 644126. https://doi.org/10.3389/fncel.2021.644126.

57. Zdebik, A.A., Wangemann, P., and Jentsch, T.J. (2009). Potassium ion movement in the inner ear: insights from genetic disease and mouse models. Physiology *24*, 307–316. https://doi.org/10.1152/physiol.00018.2009.

58. Prelic, S., Pal Mahadevan, V., Venkateswaran, V., Lavista-Llanos, S., Hansson, B.S., and Wicher, D. (2021). Functional interaction between Drosophila olfactory sensory neurons and their support cells. Front. Cell. Neurosci. *15*, 789086. https://doi.org/10.3389/fncel.2021.789086.

59. Singh, N.A., Charlier, C., Stauffer, D., DuPont, B.R., Leach, R.J., Melis, R., Ronen, G.M., Bjerre, I., Quattlebaum, T., Murphy, J.V., et al. (1998). A novel potassium channel gene, KCNQ2, is mutated in an inherited epilepsy of newborns. Nat. Genet. *18*, 25–29. https://doi.org/10.1038/ng0198-25.

60. Epi4K Consortium; Epilepsy Phenome/Genome Project, Allen, A.S., Berkovic, S.F., Cossette, P., Delanty, N., Dlugos, D., Eichler, E.E., Epstein, M.P., Glauser, T., Goldstein, D.B., Han, Y., et al. (2013). De novo mutations in epileptic encephalopathies. Nature *501*, 217–221. https://doi.org/10.1038/nature12439.

61. Kato, M., Yamagata, T., Kubota, M., Arai, H., Yamashita, S., Nakagawa, T., Fujii, T., Sugai, K., Imai, K., Uster, T., et al. (2013). Clinical spectrum of early onset epileptic encephalopathies caused by KCNQ2 mutation. Epilepsia *54*, 1282–1287. https://doi.org/10.1111/epi.12200.

62. Deciphering Developmental Disorders Study (2017). Prevalence and architecture of de novo mutations in developmental disorders. Nature *542*, 433–438. https://doi.org/10.1038/nature21062.

63. Nascimento, F.A., and Andrade, D.M. (2016). Myoclonus epilepsy and ataxia due to potassium channel mutation (MEAK) is caused by heterozygous KCNC1 mutations. Epileptic Disord. *18*, 135–138. https://doi.org/10.1684/epd.2016.0859.

64. Sontheimer, H. (1994). Voltage-dependent ion channels in glial cells. Glia *11*, 156–172. https://doi.org/10.1002/glia.440110210.

65. Wang, W., Gao, X.F., Xiao, L., Xiang, Z.H., and He, C. (2011). K(V)7/KCNQ channels are functionally expressed in oligodendrocyte progenitor cells. PLoS One *6*, e21792. https://doi.org/10.1371/journal.pone.0021792.

66. Vay, S.U., Flitsch, L.J., Rabenstein, M., Monière, H., Jakovcevski, I., Andjus, P., Bijelic, D., Blaschke, S., Walter, H.L., Fink, G.R., et al. (2020). The impact of hyperpolarization-activated cyclic nucleotide-gated (HCN) and voltage-gated potassium KCNQ/Kv7 channels on primary microglia function. J. Neuroinflammation *17*, 100. https://doi.org/10.1186/s12974-020-01779-4.

67. Wu, K.C., Kuo, C.S., Chao, C.C., Huang, C.C., Tu, Y.K., Chan, P., and Leung, Y.M. (2015). Role of voltage-gated K(+) channels in regulating Ca(2+) entry in rat cortical astrocytes. J. Physiol. Sci. *65*, 171–177. https://doi.org/10.1007/s12576-015-0356-9.

68. Blanz, J., Schweizer, M., Auberson, M., Maier, H., Muenscher, A., Hübner, C.A., and Jentsch, T.J. (2007). Leukoencephalopathy upon disruption of the chloride channel ClC-2. J. Neurosci. *27*, 6581–6589. https://doi.org/10.1523/JNEUROSCI.0338-07.2007.

69. Depienne, C., Bugiani, M., Dupuits, C., Galanaud, D., Touitou, V., Postma, N., van Berkel, C., Polder, E., Tollard, E., Darios, F., et al. (2013). Brain white matter oedema due to ClC-2 chloride channel deficiency: an observational analytical study. Lancet Neurol. *12*, 659–668. https://doi.org/10.1016/S1474-4422(13)70053-X.

70. Sík, A., Smith, R.L., and Freund, T.F. (2000). Distribution of chloride channel-2-immunoreactive neuronal and astrocytic processes in the hippocampus. Neuroscience *101*, 51–65. https://doi.org/10.1016/s0306-4522(00)00360-2.

71. Qu, Z., and Hartzell, H.C. (2008). Bestrophin Cl- channels are highly permeable to HCO3. Am. J. Physiol. Cell Physiol. *294*, C1371–C1377. https://doi.org/10.1152/ajpcell.00398.2007.

72. Rehan, S., Shahid, S., Salminen, T.A., Jaakola, V.P., and Paavilainen, V.O. (2019). Current progress on equilibrative nucleoside transporter function and inhibitor design. SLAS Discov. *24*, 953–968. https://doi.org/10.1177/2472555219870123.

73. Sheth, S., Brito, R., Mukherjea, D., Rybak, L.P., and Ramkumar, V. (2014). Adenosine receptors: expression, function and regulation. Int. J. Mol. Sci. *15*, 2024–2052. https://doi.org/10.3390/ijms15022024.

74. Sebastião, A.M., and Ribeiro, J.A. (2000). Fine-tuning neuromodulation by adenosine. Trends Pharmacol. Sci. *21*, 341–346. https://doi.org/10.1016/s0165-6147(00)01517-0.

75. de Mendonça, A., and Ribeiro, J.A. (2001). Adenosine and synaptic plasticity. Drug Dev. Res. *52*, 283–290.

76. Engel, K., Zhou, M., and Wang, J. (2004). Identification and characterization of a novel monoamine transporter in the human brain. J. Biol. Chem. *279*, 50042–50049. https://doi.org/10.1074/jbc.M407913200.

77. Sangaletti, R., Dahl, G., and Bianchi, L. (2014). Mechanosensitive unpaired innexin channels in C. elegans touch neurons. Am. J. Physiol. Cell Physiol. *307*, C966–C977. https://doi.org/10.1152/ajpcell.00246.2014.

78. Walker, D.S., and Schafer, W.R. (2020). Distinct roles for innexin gap junctions and hemichannels in mechanosensation. Elife *9*, e50597. https://doi.org/10.7554/eLife.50597.

79. Altun, Z.F., Chen, B., Wang, Z.W., and Hall, D.H. (2009). High resolution map of Caenorhabditis elegans gap junction proteins. Dev. Dynam. *238*, 1936–1950. https://doi.org/10.1002/dvdy.22025.

80. Sulston, J.E., Schierenberg, E., White, J.G., and Thomson, J.N. (1983). The embryonic cell lineage of the nematode Caenorhabditis elegans. Dev. Biol. *100*, 64–119.

81. Brenner, S. (1974). The genetics of Caenorhabditis elegans. Genetics *77*, 71–94.

82. Consortium, C.e.D.M. (2012). large-scale screening for targeted knockouts in the Caenorhabditis elegans genome. G3 *2*, 1415–1425. https://doi.org/10.1534/g3.112.003830.

83. Elkes, D.A., Cardozo, D.L., Madison, J., and Kaplan, J.M. (1997). EGL-36 Shaw channels regulate C. elegans egg-laying muscle activity. Neuron *19*, 165–174. https://doi.org/10.1016/s0896-6273(00)80356-6.

84. Mano, I., Straud, S., and Driscoll, M. (2007). Caenorhabditis elegans glutamate transporters influence synaptic function and behavior at sites distant from the synapse. J. Biol. Chem.282, 34412–34419. https://doi.org/10.1074/jbc.M704134200.

85. Colbert, H.A., and Bargmann, C.I. (1995). Odorant-specific adaptation pathways generate olfactory plasticity in C. elegans. Neuron *14*, 803–812. https://doi.org/10.1016/0896-6273(95)90224-4.

86. Hodgkin, J. (1999). Sex, cell death, and the genome of C. elegans. Cell *98*, 277–280. https://doi.org/10.1016/s0092-8674(00)81956-x.

87. Tavernarakis, N., Wang, S.L., Dorovkov, M., Ryazanov, A., and Driscoll, M. (2000). Heritable and inducible genetic interference by double-stranded RNA encoded by transgenes. Nat. Genet. *24*, 180–183. https://doi.org/10.1038/72850.

88. Mello, C.C., Kramer, J.M., Stinchcomb, D., and Ambros, V. (1991). Efficient gene transfer in C.elegans: extrachromosomal maintenance and integration of transforming sequences. EMBO J. *10*, 3959–3970.

89. Loria, P.M., Hodgkin, J., and Hobert, O. (2004). A conserved postsynaptic transmembrane protein affecting neuromuscular signaling in Caenorhabditis elegans. J. Neurosci. *24*, 2191–2201. https://doi.org/10.1523/JNEUROSCI.5462-03.2004.

90. Melentijevic, I., Toth, M.L., Arnold, M.L., Guasp, R.J., Harinath, G., Nguyen, K.C., Taub, D., Parker, J.A., Neri, C., Gabel, C.V., et al. (2017). C. elegans neurons jettison protein aggregates and mitochondria under neurotoxic stress. Nature *542*, 367–371. https://doi.org/10.1038/nature21362.

91. Katz, M., Corson, F., Keil, W., Singhal, A., Bae, A., Lu, Y., Liang, Y., and Shaham, S. (2019). Glutamate spillover in C. elegans triggers repetitive behavior through presynaptic activation of MGL-2/mGluR5. Nat. Commun. *10*, 1882. https://doi.org/10.1038/s41467-019-09581-4.

92. Fernandez-Abascal, J., and Bianchi, L. (2022). A protocol for imaging calcium and chloride in C. elegans glia upon touch stimulation. STAR Protoc. *3*, 101282. https://doi.org/10.1016/j.xpro.2022.101282.

93. Ikenaka, K., Tsukada, Y., Giles, A.C., Arai, T., Nakadera, Y., Nakano, S., Kawai, K., Mochizuki, H., Katsuno, M., Sobue, G., and Mori, I. (2019). A behavior-based drug screening system using a Caenorhabditis elegans model of motor neuron disease. Sci. Rep. *9*, 10104. https://doi.org/10.1038/s41598-019-46642-6.

STAR★METHODS

KEY RESOURCES TABLE

REAGENT or RESOURCE	SOURCE	IDENTIFIER
Bacterial and virus strains		
Escherichia coli	CGC	*OP50*
Chemicals, peptides, and recombinant proteins		
Octanol	Sigma-Aldrich	Cat#112615
Glycerol	Sigma-Aldrich	Cat#G5516
Isoamyl alcohol	Sigma-Aldrich	Cat#AX1440
Na-acetate	Sigma-Aldrich	Cat#S2889
Diacetyl	Sigma-Aldrich	Cat#B0682
Ethyl alcohol	Pharmco	Cat#111000200
Chloroform	Sigma-Aldrich	Cat#C2432
Dimethyl sulfoxide	Sigma-Aldrich	Cat#D5879
Bicuculline	VWR	Cat#TBC1890
α-MDG	Sigma-Aldrich	Cat#102987-308
Nifedipine	Thomas Scientific	Cat#C931M79
KCl	Sigma-Aldrich	Cat#9541
NaN_3	Sigma-Aldrich	Cat#S2002
Gluture	Fisher Scientific	Cat#NC0632797
Experimental models: Organisms/strains		
N2	CGC[81]	N2
clh-3(ok768)	CGC[82]	RB905
egl-36(n728n398)	CGC[83]	KP1008
ent-4(ok2161)	CGC[82]	VC1934
glc-3(ok321)	CGC[82]	RB594
glt-5(bz70)	CGC[84]	ZB1099
glt-5(ok1987)	CGC[82]	RB1615
gtl-1(ok375)	CGC[82]	VC244
kcc-1(ok648)	CGC[82]	VC476
kcc-1(ok692)	CGC[82]	VC542
tax-2(p691)	CGC[36]	PR691
kqt-2(ok732)	CGC[82]	RB883
nsIs109 [F16F9.3p::DTA(G53E) +unc-122p::GFP]	CGC[16]	OS2248
odr-3(n2150)	CGC[85]	CX2205
kyIs722 [str-2p::GCaMP5(D380Y) + elt-2::mCherry]	CGC	CX17256
kqt-2(tm642)	NBRP	N/A
best-9(tm7876)	NBRP	N/A
Ex[PT02B11.3::abts-4 RNAi + unc-122p::GFP + Pvap-1::RFP]	This study	BLC340
Ex[PT02B11.3::best-9 RNAi + unc-122p::GFP + Pvap-1::RFP]	This study	BLC342

(*Continued on next page*)

Continued

REAGENT or RESOURCE	SOURCE	IDENTIFIER
Ex[PT02B11.3::clh-3 RNAi + unc-122p::GFP + Pvap-1::RFP]	This study	BLC337
Ex[PT02B11.3::egl-36 RNAi + unc-122p::GFP + Pvap-1::RFP]	This study	BLC336
Ex[PT02B11.3::glc-3 RNAi + unc-122p::GFP + Pvap-1::RFP]	This study	BLC345
Ex[PT02B11.3::kcc-1 RNAi + unc-122p::GFP + Pvap-1::RFP]	This study	*BLC329*
Ex[PT02B11.3::twk-21 RNAi + unc-122p::GFP + Pvap-1::RFP]	This study	BLC350
Ex[PT02B11.3::twk-33 RNAi + unc-122p::GFP + Pvap-1::RFP]	This study	BLC338
Ex[PT02B11.3:kqt-2 RNAi + unc-122p::GFP + Pvap-1::RFP]	This study	BLC358
Ex[pSra-6::GCaMP-6s + unc-122::GFP]	This study	BLC400
clh-3(ok768);Ex[PT02B11.3::clh-3b cDNA + Punc-122::GFP]	This study	BLC356
kcc-1(ok648);Ex[PT02B11.3::SLC12A4 + Punc-122::GFP]	This study	BLC547
best-9(tm7876);Ex[PT02B11.3::best-9 cDNA + Punc-122::GFP]	This study	BLC551
egl-36(n728n398);Ex[PT02B11.3::egl-36 cDNA + Punc-122::GFP]	This study	BLC552
ent-4(ok2161);Ex[PT02B11.3::ent-4 cDNA + Punc-122::GFP]	This study	BLC555
kqt-2(ok732);Ex[PT02B11.3::kqt-2 cDNA + Punc-122::GFP]	This study	BLC491
Ex[PT02B11.3::unc-25 RNAi + unc-122p::GFP]	This study	BLC500
best-9(tm7876);[osm-10::GFP + lin-15(+)]	This study	BLC554
clh-3(ok768); [gcy-5p::GFP + lin-15(+)]	This study	BLC553
clh-3(ok768);[osm-10::GFP + lin-15(+)]	This study	BLC548
clh-3(ok768);[str-2::GFP + lin-15(+)]	This study	BLC550
egl-36(n728n398);[osm-10::GFP + lin-15(+)]	This study	BLC556
egl-36(n728n398);[str-2::GFP + lin-15(+)]	This study	BLC560
ent-4(ok2161);[osm-10::GFP + lin-15(+)]	This study	BLC557
kcc-1(ok648);[osm-10::GFP + lin-15(+)]	This study	BLC558
kcc-1(ok648);[str-2::GFP + lin-15(+)]	This study	BLC561
kqt-2(ok732);[osm-10::GFP + lin-15(+)]	This study	BLC559
best-9(tm7876);Ex[PT02B11.3::GCaMP6s + Punc-122::GFP]	This study	BLC562
clh-3(ok768);Ex[PT02B11.3::GCaMP6s + Punc-122::GFP]	This study	BLC563
egl-36(n728n398);Ex[PT02B11.3::GCaMP6s + Punc-122::GFP]	This study	BLC564
ent-4(ok2161);Ex[PT02B11.3::GCaMP6s + Punc-122::GFP]	This study	BLC566
kcc-1(ok648);Ex[PT02B11.3::GCaMP6s + Punc-122::GFP]	This study	BLC565

(*Continued on next page*)

Continued

REAGENT or RESOURCE	SOURCE	IDENTIFIER
kqt-2(ok732);Ex[PT02B11.3::GCaMP6s + Punc-122::GFP]	This study	BLC567
best-9(tm7876);Ex[PT02B11.3::GCaMP6s + Punc-122::GFP]	This study	BLC568
egl-36(n728n398);Ex[pSra-6::GCaMP-6s + unc-122::GFP]	This study	BLC570
ent-4(ok2161);Ex[pSra-6::GCaMP-6s + unc-122::GFP]	This study	BLC572
kcc-1(ok648);Ex[pSra-6::GCaMP-6s + unc-122::GFP]	This study	BLC573
kqt-2(ok732);Ex[pSra-6::GCaMP-6s + unc-122::GFP]	This study	BLC 492
best-9(tm7876);Ex[pSra-6::GCaMP-6s + unc-122::GFP]	This study	BLC572
egl-36(n728n398);Ex[pSra-6::GCaMP-6s + unc-122::GFP]	This study	BLC577
ent-4(ok2161);Ex[pSra-6::GCaMP-6s + unc-122::GFP]	This study	BLC578
kcc-1(ok648);Ex[pSra-6::GCaMP-6s + unc-122::GFP]	This study	BLC579
clh-3(ok768);[str-2p::GCaMP5(D380Y) + elt-2::mCherry]	This study	BLC574
egl-36(n728n398);[str-2p::GCaMP5(D380Y) + elt-2::mCherry]	This study	BLC524
kcc-1(ok648);[str-2p::GCaMP5(D380Y) + elt-2::mCherry]	This study	BLC575
clh-3(ok768);Ex[PT02B11.3::clh-3b cDNA + Punc-122::GFP];[str-2p::GCaMP5(D380Y) + elt-2::mCherry]	This study	BLC583
egl-36(n728n398);Ex[PT02B11.3::egl-36 cDNA + Punc-122::GFP];[str-2p::GCaMP5(D380Y) + elt-2::mCherry]	This study	BLC584
kcc-1(ok648);Ex[PT02B11.3::SLC12A4 + Punc-122::GFP];[str-2p::GCaMP5(D380Y) + elt-2::mCherry]	This study	BLC585
best-9(tm7876);Ex[pSra-6::GCaMP-6s + unc-122::GFP + PT02B11.3::best-9 cDNA + Pmec-4::mcherry]	This study	BLC587
egl-36(n728n398);Ex[pSra-6::GCaMP-6s + unc-122::GFP + PT02B11.3::egl-36 cDNA + Pmec-4::mcherry]	This study	BLC588
ent-4(ok2161);Ex[pSra-6::GCaMP-6s + unc-122::GFP + PT02B11.3::ent-4 cDNA Pmec-4::mcherry]	This study	BLC580
kcc-1(ok648);Ex[pSra-6::GCaMP-6s + unc-122::GFP + PT02B11.3::SLC12A4 cDNA + Pmec-4::mcherry]	This study	BLC581
kqt-2(ok732);Ex[pSra-6::GCaMP-6s + unc-122::GFP + PT02B11.3::kqt-2 cDNA + Pmec-4::mcherry]	This study	BLC582

(*Continued on next page*)

Continued

REAGENT or RESOURCE	SOURCE	IDENTIFIER
kcc-1(ok648);Ex[pSra-6::GCaMP-6s + unc-122::GFP + PT02B11.3::kcc-1a cDNA + Pmec-4::mcherry]	This study	BLC648
kcc-1(ok648);Ex[pSra-6::GCaMP-6s + unc-122::GFP + Pstr-2::kcc-1a cDNA + Pmec-4::mcherry]	This study	BLC649
best-9(tm7876);Ex [pT02B11.3::SuperClomeleon]	This study	BLC616
kcc-1(ok648);Ex[pT02B11.3::SuperClomeleon]	This study	BLC628
clh-3(ok768);Ex[pT02B11.3::SuperClomeleon]	This study	BLC621
Ex[pT02B11.3::SuperClomeleon]	This study	BLC498
best-9(tm7876);Ex[PT02B11.3::kcc-1 RNAi + unc-122p::GFP + Pvap-1::RFP]	This study	BLC567
kqt-2(ok732);Ex[PT02B11.3::egl-36 RNAi + unc-122p::GFP + Pvap-1::RFP]	This study	BLC571
clh-3(ok768);kcc-1(ok648)	This study	BLC605
Ex[PT02B11.3:egl-19 RNAi + unc-122p::GFP]	This study	BLC630
Oligonucleotides		
pPD95_75	A gift from Andrew Fire	RRID:Addgene_1494
pPD95_75 (pSra-6::::GCaMP-6s)	This study	N/A
pPD95_75 (pT02B11.3::SLC12A4)	This study	N/A
pPD95_75 (pT02B11.3::clh-3b cDNA)	This study	N/A
pPD95_75 (pT02B11.3::kcc-1a cDNA)	This study	N/A
pPD95_75 (pstr-2::kcc-1a cDNA)	This study	N/A
pPD95_75 (pT02B11.3::sense kcc-1 RNAi)	This study	N/A
pPD95_75 (pT02B11.3::antisense kcc-1 RNAi)	This study	N/A
pPD95_75 (pT02B11.3::sense abts-4 RNAi)	This study	N/A
pPD95_75 (pT02B11.3::antisense abts-4 RNAi)	This study	N/A
pPD95_75 (pT02B11.3::sense best-9 RNAi)	This study	N/A
pPD95_75 (pT02B11.3::antisense best-9 RNAi)	This study	N/A
pPD95_75 (pT02B11.3::sense clh-3 RNAi)	This study	N/A
pPD95_75 (pT02B11.3::antisense clh-3 RNAi)	This study	N/A
pPD95_75 (pT02B11.3::sense egl-36 RNAi)	This study	N/A
pPD95_75 (pT02B11.3::antisense egl-36 RNAi)	This study	N/A
pPD95_75 (pUnc-122::GFP)	(Grant et al., 2015)[20]	N/A
pPD95_75 (pVap-1::RFP)	(Johnson et al., 2020)[22]	N/A
pPD95_75 (pT02B11.3::sense glc-3 RNAi)	This study	N/A
pPD95_75 (pT02B11.3::antisense glc-3 RNAi)	This study	N/A
pPD95.75 (pT02B11.3::sense twk-33 RNAi)	This study	N/A
pPD95.75 (pT02B11.3::antisense twk-33 RNAi)	This study	N/A
pPD95_75 (pT02B11.3::SuperClomeleon)	This study	N/A
pPD95_75 (pT02B11.3::sense twk-21 RNAi)	This study	N/A
pPD95_75 (pT02B11.3::antisense twk-21 RNAi)	This study	N/A
pPD95_75 (pT02B11.3::sense kqt-2 RNAi)	This study	N/A
pPD95_75 (pT02B11.3::antisense kqt-2 RNAi)	This study	N/A
pPD95_75 (pT02B11.3::best-9 cDNA)	This study	N/A

(*Continued on next page*)

Continued

REAGENT or RESOURCE	SOURCE	IDENTIFIER
pPD95_75 (pT02B11.3::ent-4 cDNA)	This study	N/A
pPD95_75 (pT02B11.3::kqt-2 cDNA)	This study	N/A
pMec-4::mcherry	This study	N/A
pT02B11.3::sense egl-19 RNAi	This study	N/A
pT02B11.3::antisense egl-19 RNAi	This study	N/A
Software and algorithms		
Fiji (ImageJ)	NIH	http://fiji.sc RRID:SCR_002285
Micro-manager	Vale Lab, UCSF	https://micro-manager.org/ RRID:SCR_000415
RStudio	RStudio	http://www.rstudio.com/ RRID:SCR_000432
GraphPad Prism	GraphPad software	http://www.graphpad.com/ RRID:SCR_002798

RESOURCE AVAILABILITY

Lead contact

Further information and requests for resources should be directed to and will be fulfilled by the Lead Contact, Laura Bianchi (l.bianchi@med.miami.edu).

Materials availability

This study did not generate any new unique reagent.

Data and code availability

- Original data reported in this paper will be shared by the lead contact upon request.
- This paper does not report original code.
- Any additional information required to reanalyze the data reported in this paper is available from the lead contact upon request.

EXPERIMENTAL MODEL AND SUBJECT DETAILS

C. elegans

Nematode strains were maintained at 20°C on standard nematode growth medium (NGM) seeded with *Escherichia coli* strain *OP50*.[81] The worms were tested when they reached the young adult stage (day 1 adults). The strains listed above and labeled with BLC were generated by injecting the corresponding DNA constructs. The crosses were carried out as described.[86] The primers used for confirm the genotype of crosses are listed in Table S1. Crosses using *egl-36(n728n398)* were confirmed by counting the number of eggs laid the first day of adult and by attraction index to isoamyl alcohol. BLC587, BLC588, BLC580, BLC581, BLC582, BLC648, and BLC649 were generated by injection of the rescue plasmid into the corresponding GCaMP strains, using *Pmec-4::mcherry* as contransformation marker. Growth of worms on plates containing 150 mM alpha-methyl-D-glucopyranose (α-MDG) or 150 mM KCl was carried out as previously described.[22,24] To avoid inconsistencies in the growth of the *E. coli* on α-MDG or KCl supplemented plates, the *OP50* was concentrated by centrifugation at 3000 rpm for 15 min and then seeded onto the plates. After the *OP50* was dry, synchronized eggs were seeded on the control and α-MDG or KCl supplemented plates. Randomly selected worms were then used for quantification of body and ASH cilia size, for Ca^{2+} imaging, or behavioral assays.

METHODS DETAILS

Molecular biology

The RNAi strains were generated following standard procedures with minor modifications.[87] Briefly, The RNAi constructs were built using the pPD95.75 vector as backbone in which the Amsh glia promoter

T02B11.3 was inserted using SphI and Acc65I restriction sites, as previously described.[17] Following the promoter sequence, a sense and, separately, an antisense 400–700 bp long sequence corresponding to an exon rich region of genomic DNA was inserted. The primers used for the amplification of sense and antisense constructs are listed in Table S1. Following DNA purification by Sigma columns, sense and antisense DNA constructs were micro-injected in the gonadal syncytia at the concentration of 50 μg/μL each.[88] The *egl-19* RNAi strain was generated by using double strand DNA fragment of Amsh glia promoter T02B11.3 and 570 bp of sense and antisense *egl-19* fragment generated by overlapping PCR. Amsh glial marker *vap-1p*::RFP[16]} and co-injection marker *unc-122p*::GFP[89] were also co-injected at the concentration of 25 μg/μL. To build rescue strains we used the same pPD95.75 plasmid containing the Amsh glia promoter T02B11.3 used for the RNAi strains. In this case, the cDNA corresponding to each gene (*kqt-2, best-9*, *clh-3b, ent-4b, kcc-1a*) was amplified by RT-PCR (primers listed in Table S1) and cloned downstream of the T02B11.3 promoter. To rescue *kcc-1* and *egl-36* we used the cDNA corresponding to human KCC1 worm *kcc-1a*, and *egl-36* respectively (pDONR221_SLC12A4 clone, *C. elegans* cDNA library, #131932 and poX_Shaw2 clone, #16114 from Addgene). Rescue constructs were injected at the concentration of 50 ug/uL. The coelomocytes marker *Punc-122::GFP* was co-injected at the concentration of 25 μg/μL to generate all the rescue strains used for behavioral assays. For the rescue strains used for ASH calcium imaging, the co-transformation marker *Pmec-4::mcherry*[90] at the concentration of 25 ug/uL and the rescue construct at the concentration of 50 μg/μL were used. Injection of these DNA constructs was done into the mutant strains expressing *Psra-6:GCaMP-6s.* For the strains used for Amsh glia chloride imaging, the *kcc-1(ok648)*, *clh-3(ok768)*, and *best-9(tm7876)* mutants were crossed with the *Ex*[*pT02B11.3::SuperClomeleon*] strain. For the rescue strains used for AWC calcium imaging, the knockout strains were crossed with the *pstr-2:GCaMP5(D380Y)* strain then injected with the co-transformation marker *Punc-122::GFP* at the concentration of 25 μg/μL and the rescue construct at the concentration of 50 μg/μL. For the *kcc-1* AWC rescue strain, the *kcc-1(ok648);[pstr-2::GCaMP5(D380Y) + elt-2::mCherry]* strain was injected with the co-transformation marker *Punc-122::GFP* at the concentration of 25 ug/uL and the rescue construct at the concentration of 50 μg/μL. Worms expressing both GFP and RFP markers were selected for chemotaxis assay and calcium imaging.

Comparison of gene-expression

For comparisons of gene expression, RNA-sequencing and DNA microchip data from other three *C. elegans* Amsh cells datasets were used.[16,25,26] The log2 number of transcripts per million reads, and fold enrichment (FE) values were calculated as previously described.[91]WormBase gene ID number was used as a unique identifier for *C. elegans* genes. To generate a volcano plot of Amsh glia-expressed genes,[20] FE values in each list were used and the volcano plot was generated using ggplot2 package of R software (https://cran.r-project.org/web/packages/ggplot2).

Behavioral assays

For chemotaxis and avoidance assays we followed previously described procedures.[27–29,42] For isoamyl alcohol and diacetyl assays, 3 μL of odorant at the indicated dilution was placed on one side of the plate. For Na-acetate assays, a chunk of agar 1-cm in diameter was removed from 10-cm plates and soaked in the attractant for 3 h. Chunks were put back in the plate overnight to allow equilibration and formation of a gradient. Fifty microliters of 100 mM NaN_3 was placed on both the control and the test spots to anesthetize animals once they reached the spot. Thirty worms were then placed between the test spot and a control spot on the opposite side of the plate. After 1 h, animals on each side of the plate were counted and the Attraction Index was calculated as follows: (number of animals at attractant — number of animals at control)/(total number of animals). For octanol avoidance assays we dipped an eyelash hair glued on a toothpick in 10% octanol and we placed in front of a forward moving animal on a plate with a thin layer of bacteria. We measured the time it took for the animal to respond to the odorant by reversing direction.[42] Odorants were diluted in ethanol. All behavioral assays were performed blind to the genotype. For octanol avoidance adaptation assays adult worms were transferred onto a 2.5 cm-diameter NGM plate and 5 μL of undiluted octanol was applied on the lid which was then sealed with Parafilm. After 5-min adaptation, animals were collected and washed twice with basal buffer (5 mm KPO_4 [pH 6], 1 mm $CaCl_2$, 1 mm $MgSO_4$) in a 1.5 mL tube and then transferred onto seeded NGM plates. Avoidance assays were performed after 30 min.

For nose touch avoidance assays young adults were transferred onto plates containing a thin layer of *OP50* bacteria and allowed to recover for 30 min. An eyelash was placed perpendicular to a forward-moving animal and a positive response was recorded if the animal reversed direction or moved the head away from the eyelash upon contact with the eyelash. A no response was recorded when the worm continued its

forward movement to crawl under, above, or along the eyelash.[24,37] Nose-touch insensitive *trpa-1*mutant was used as control.[37] Each worm was tested for 5 consecutive times with a ~30 s interval. At least 10 worms per strain were tested in each assay. The average positive response of each worm to the 5 touches was then used to calculate the average response of each strain. For octanol avoidance and nose touch assays, experiments were performed blind to the genotype.

Fluorescence and confocal microscopy

To measure the size of wild type, *kcc-1*, and *clh-3*mutant worms, randomly selected fluorescent/expressing GCaMP-6s worms were anesthetized with 100 mM NaN_3 and arranged on a 2% agar (in M9 buffer) pad for each group. To quantify Amsh glia morphology, the EVOS FL auto 2 system was used and stacks of fluorescent images with 3 μm spacing were taken using a 10X and 40× objective. To quantify the size of the cilia in AWC and ASE neurons, fluorescent images were acquired using a Zeiss Axio Observer microscope equipped with an ORCA-Flash 4.0 V2 digital CMOS camera using a 63× water objective. The HCImage acquisition software was used to take the images, that were then processed with Fiji (ImageJ) software. To determine the size of the cilia of ASH neurons, images were taken with an Olympus IX81 confocal microscope equipped with an 60× oil immersion objective (Olympus) using a 488 nm laser (10% intensity). The scan speed was set as 8.0 μs per pixel and the spatial resolution was set as 1024 × 1024 pixels. To visualize the cilia, a 9.5 digital zoom was used with an average of around 20 "Z" stacks with 0.3 μm step size for AWC samples and around 10 "Z" stacks with 0.5 μm step size for ASH samples. The Images were further analyzed with "Z project" maximum intensity function of Fiji (ImageJ software). The area and length of ASH and area of AWC cilia were measured in the merged images.

Calcium imaging

Calcium imaging recordings were performed following standard procedure with minor modifications.[24,92] The calcium sensor GCaMP-6s was used for recordings of Amsh cells and ASH neurons. The calcium sensor GCaMP5 was used for recordings of AWC neurons. One-day-old adults were glued onto 2% agarose pads prepared using extracellular saline solution (145 mM NaCl, 5 mM KCl, 1 mM $CaCl_2$, 5 mM $MgCl_2$, 20 mM D-glucose, 10 mM HEPES buffer, pH 7.2) using Gluture (Fisher Scientific, #NC0632797) and immersed in the same solution, as previously described.[18,19,24,92]octanol and IAA were dissolved 1:1 using DMSO and then diluted in the perfusion buffer. The solution was vortexed each time before use and delivered to a recording chamber (1156 mm^3) via gravity perfusion; the speed of perfusion was 10 mL per mins. The chamber was mounted on an Olympus IX70 microscope with anX10 objective (Olympus) and a PCO SensiCam camera. The microscope was equipped with a Lambda DG-4 illumination system (Sutter Instrument Co.) as a light source and excitation filter FF01-500/24–25 (Semrock) to monitor GCaMP fluorescence. Images were acquired using Micro-Manager 2.0 software[93] at a frequency of 1 Hz with 100 ms exposure time and a spatial resolution of 1024x1024 pixels. Basal fluorescence was acquired for 10 s prior to the perfusion with the odorant. The perfusion with the odorants and Na-acetate was for 30 s, followed by wash with the control perfusion solution until the end of the recording. The fluorescence intensity was calculated by subtracting the background. The background was obtained by selecting a small region of the worm body near the imaged cell and by calculating its average fluorescence across the entire recording. Images were analyzed using Fiji (ImageJ) and plotted using GraphPad Prism (version 8.4.2). Data were normalized using the average fluorescence corresponding to the 10 s before the perfusion with the odorants and Na-acetate.

For experiments using bicuculline we followed previously reported procedures.[23,24] Briefly, 100 μL of bicuculline at the concentration of 10 mM (in 0.1% chloroform) was spread on an NGM plate and let dry before a layer of bacteria was seeded on the agar. The control plate was prepared similarly but using chloroform only. For experiments using Nifedipine, previously reported procedures with minor modifications were followed.[93] Briefly, 2 μL of Nifedipine at the concentration of 100 mM in 100% DMSO was added to 2 mL of S medium (100 mM NaCl, 5.7 mM K_2HPO_4, 44 mM KH_2PO_4, 12.9 μM cholesterol) containing 5 mg/mL of *OP50* and then transferred into a 35 mm Petri dish. The control group used 2 μL of DMSO instead. The worms were allowed to crawl for 30 min before the calcium imaging experiments.

Chloride imaging

Chloride imaging was carried out as previously described.[23,24,92] The change of chloride concentration was determined using the YFP/CFP FRET-based chloride sensor SuperClomeleon. Briefly, the excitation filter FF02-438/24 (Semrock) was used to excite the sensor and the emission filters FF01-483/32 and

FF01-542/27 were used to capture CFP and YFP fluorescence, respectively, for 180 s. The fluorescence intensity of each channel of glial cell body was calculated by subtracting the background intensity. Then, the ratio YFP/CFP (R) was calculated for each frame accordingly. The average ratio of the 10 s (R_0) before stimulation was considered as basal level. The following YFP/CFP ratios were calculated by comparing the difference with the average basal level of the 10 s (R/R_0) before stimulation.

QUANTIFICATION AND STATISTICAL ANALYSIS

To determine significance between two groups, unpaired two-sided student's Test was used. For multiple groups, one way ANOVA with Tukey correction was used. All the analyses were performed using GraphPad Prism 9. The specific test used, and the pvalues are indicated in the Figure legends. Data are shown as individual data points and as mean $\pm$ SE.